Science Advances
AAAS

Supplementary Materials for

Meniscal fibrocartilage regeneration inspired by meniscal maturational and regenerative process

Wenqiang Yan *et al.*

Corresponding author: Yingfang Ao, aoyingfang@163.com; Jin Cheng, chengjin@bjmu.edu.cn; Xiaoqing Hu, huxiaoqingbd01@sina.com

Sci. Adv. **9**, eadg8138 (2023)
DOI: 10.1126/sciadv.adg8138

The PDF file includes:

Other Supplementary Material for this manuscript includes the following:

Results

3D printing meniscal regeneration scaffold

Medial menisci **(Supplemental Fig. 27A1)** were harvested from a male minipig cadaver. 2D images were obtained by micro-CT scanning **(Supplemental Fig. 27A2)**. The 3D model of native meniscus was constructed **(Supplemental Fig. 27A3, A4)**. The bottom of native meniscus was not flat. However, a lot of published studies of 3D printing meniscal scaffold constructed flat bottom (*9, 45, 46*). The flat bottom did not match native morphology of tibial plateau. In order to highlight the advantage of supporting printing in constructing native morphology of meniscus. Another meniscal model with flat bottom was constructed **(Supplemental Fig. 27A5, A6).** The native meniscal model and flat-bottom model were imported into the bioprinter. For native meniscal model, after uniform slicing, a total of 20 layers with 320 μm thickness of each layer was identified for the main subject **(Supplemental Fig. 27A7)**. Then, a supporting model was generated. The optimal parameters of supporting model were set as: polygon offset (PO, 600 μm), layer thickness (LT, 320 μm), and detail threshold (800 μm) **(Supplemental Fig. 27B7)**. After uniform slicing for supporting model, a total of 9 layers with 320 μm thickness of each layer was identified **(Supplemental Fig. 27A8, A9)**. For flat-bottom meniscal model, after uniform slicing, a total of 14 layers with 320 μm thickness of each layer was identified **(Supplemental Fig. 27A10)**. In order to simulate native meniscal collagen fibers arrangement, the peripheral contour of each layer was printed to simulate the circumferential arrangement **(Supplemental Fig. 27B1, B2)**, and the inner structure of a cross was used to simulate the radial arrangement **(Supplemental Fig. 27B3, B4)**. The distance between strands in the inner structure was set as 1 mm. For the printing of supporting structure, the printing path

design only included the inner structure. Horizontal lines with single direction were used. The distance between strands was set as 1.2 mm **(Supplemental Fig. 27B5, B6)**.

After preparing 30% Pluronic F-127, PCL pellets and identifying optimal printing parameters **(Supplemental Fig. 27B8-B12),** the meniscal scaffold printing was performed. Firstly, the biomimetic scaffold with native bottom morphology was attempted using supporting printing **(Supplemental Movie-1)**. After layer-by-layer printing, the biomimetic meniscal scaffold was completed **(Supplemental Fig. 27C1-C4)**. Afterwards, the meniscal scaffold was immersed into water to remove Pluronic F-127 **(Supplemental Fig. 27C5)**. The surface and bottom morphology of meniscal scaffold simulated native menisci. Moreover, the PCL strands demonstrated circumferential and radial orientation simulating native collagen fiber arrangement **(Supplemental Fig. 27C6-C8)**. Secondly, the meniscal model with native bottom morphology was attempted without supporting model **(Supplemental Movie-2)**. No Pluronic F-127 strands was used to fill in the blank space. After layer-by-layer printing, the PCL strands were arranged disorderly, losing ordered circumferential and radial arrangement **(Supplemental Fig. 27D1-D5)**. Thirdly, meniscal scaffold with flat bottom was printed **(Supplemental Movie-3)**. As the bottom was flat, the PCL strands could lie on the platform at the beginning. After layer-by-layer printing, the meniscal scaffold with flat bottom was finished **(Supplemental Fig. 27E1-E5)**. However, the flat bottom morphology was against the supporting printing meniscal scaffold and native menisci **(Supplemental Fig. 27F)**. Using supporting printing, the biomimetic human meniscal scaffold could be constructed for total or partial meniscal replacement

(Supplemental Fig. 27G, H). The beagle canine meniscal scaffold could also be constructed biomimetically **(Supplemental Fig. 27I)**.

We then evaluated the morphology of native porcine medial tibial plateau. The general anatomy **(Supplemental Fig. 28A1-A4)** and 3D model **(Supplemental Fig. 28B1-B4)** showed the medial tibial plateau was not in one plane. The quantitative analysis demonstrated the vertical distances of medial intercondylar notch to anterior rim, medial rim, and posterior rim were 4.56, 6.14, and 12.96 mm, respectively. The vertical distances of anterior rim to medial rim and posterior rim were 1.67 and 7.93 mm, respectively. The vertical distance between medial rim and posterior rim was 5.41 mm **(Supplemental Fig. 28C1, C2)**. The medial tibial plateau of other species was also not flat, including human, goat, canine, and rabbit **(Supplemental Fig. 28D)**. After transplanting the supporting printing meniscal scaffold in a porcine tibia specimen, the meniscal scaffold bottom matched the morphology of tibial plateau evaluated from anterior, posterior, medial and top views **(Supplemental Fig. 28E1-E4)**. However, after transplanting the meniscal scaffold with flat bottom, the scaffold was only contacted with the prominent middle zone of tibial plateau, leaving the anterior and posterior segments suspended **(Supplemental Fig. 28F1-F4)**. We also compared the force distribution between native meniscal model and flat bottom model using finite element analysis (FEA). For native meniscal model, the outcomes of FEA demonstrated the compression was distributed relatively uniformly across the meniscus and tibial plateau, without stress concentration **(Supplemental Fig. 28G1, G2)**. However, for flat bottom model, the compression was distributed concentrating on the central body of meniscal

model and the middle prominent zone of tibia plateau **(Supplemental Fig. 28G3, G4)**. For native human knee joint, the compression was distributed relatively uniformly across the medial meniscus and medial tibial plateau, without obvious stress concentration **(Supplemental Fig. 28G5, G6)**.

The PCL material used for printing should match the native menisci in terms of mechanical properties. Firstly, the mechanical property of native porcine menisci was evaluated. The native porcine menisci were bisected into femoral and tibial aspects from the axial plane, and were further divided into anterior, central body and posterior segments **(Supplemental Fig. 29A1, A2)**. The PCL material was molded into dumbbell-shaped samples **(Supplemental Fig. 29A3)**. For the femoral surface of native porcine menisci, the shore hardness (A) of anterior segment, central body and posterior segment was 59.27±6.53, 35.77±7.83, and 77.60±2.33, respectively. For the tibial surface of native porcine menisci, the shore hardness (A) of anterior segment, central body and posterior segment was 61.33±4.31, 45.67±9.17 and 81.50±0.80, respectively. The shore hardness (A) of two commonly used PCL (Mw. 43,000-50,000 Da) and PCL (Mw. 80,000 Da) was 61.80±6.47 and 89.60±6.18, respectively **(Supplemental Fig. 29A4)**. In order to reflect the general distribution of shore hardness in native porcine meniscus visually, a heat map was used **(Supplemental Fig. 29A5)**. However, the shore hardness distribution was not uniform within each section, the mean values of shore hardness in each section were only used to assess the hardness discrepancy among sections in the present study. After the preparation of scaffold samples, the SEM was then performed **(Supplemental Fig. 29B1)**. The PCL strands demonstrated smooth

surface, relative consistent diameter, and close contact. The layer-by-layer structure was clear. The PCL strands demonstrated ordered arrangement with circumferential and radial orientation. The interspace between PCL strands was distinct and consistent **(Supplemental Fig. 29B2)**. For the cytocompatibility of PCL scaffold, after culturing for 3 days, the live-dead staining of MSCs demonstrated almost all green fluorescence, indicating live cells **(Supplemental Fig. 29C1)**. The cytoskeleton of cells demonstrated extension morphology **(Supplemental Fig. 29C2)**.

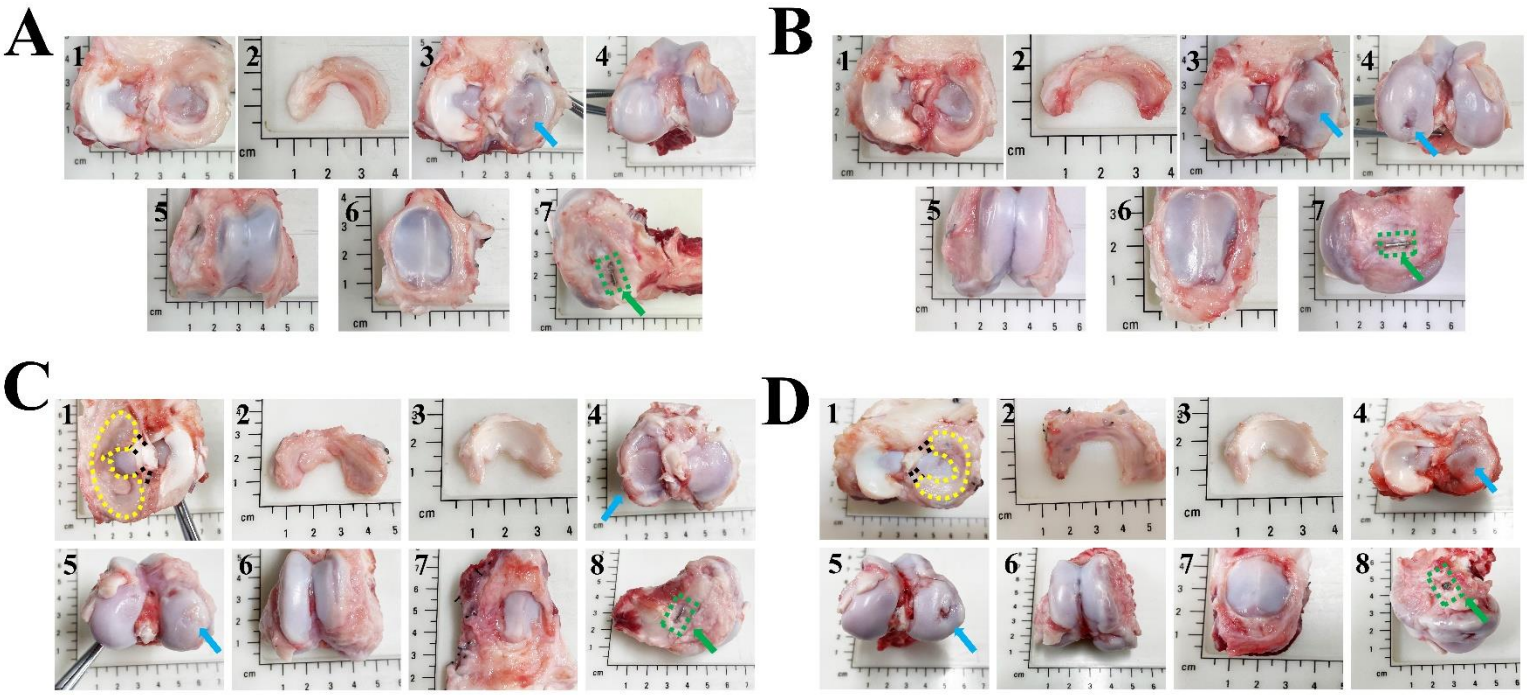
A
1
2
3
4
5
6
7
B
1
2
3
4
5
6
7
C
1
2
3
4
5
6
7
8
D
1
2
3
4
5
6
7
8

Supplemental figure 1. The macroscopic analyses of regenerated tissue of subtotal meniscectomy group and blank PCL scaffold group. (A) The macroscopic appearance of spontaneously regenerated tissue and cartilage status of subtotal meniscectomy group at 2 months postoperatively (**1,** the regenerated tissue located in the tibia; **2,** the spontaneously regenerated tissue; **3,** the tibial plateau cartilage, blue arrowhead represents cartilage wear; **4,** the femoral condyle cartilage; **5,** cartilage in the trochlea; **6,** cartilage in the patella; **7,** good bone healing of medial collateral ligament upper attachment site as indicated by green arrowhead). **(B)** The macroscopic appearance of spontaneously regenerated tissue and cartilage status of subtotal meniscectomy group at 4 months postoperatively. **(C)** The macroscopic appearance of regenerated tissue and cartilage status of blank PCL scaffold group at 2 months postoperatively (**1,** the regenerated tissue located in the tibia, black dotted lines represent anterior and posterior attachment ligament, yellow dotted line represents contour of regenerated tissue; **2,** the regenerated tissue; **3,** native meniscus; **4,** the tibial plateau cartilage; **5,** the femoral condyle cartilage, blue arrowhead represents cartilage wear; **6,** cartilage in the trochlea; **7,** cartilage in the patella; **8,** good healing of medial collateral ligament upper attachment site). **(D)** The macroscopic appearance of regenerated tissue and cartilage status of blank PCL scaffold group at 4 months postoperatively**.**

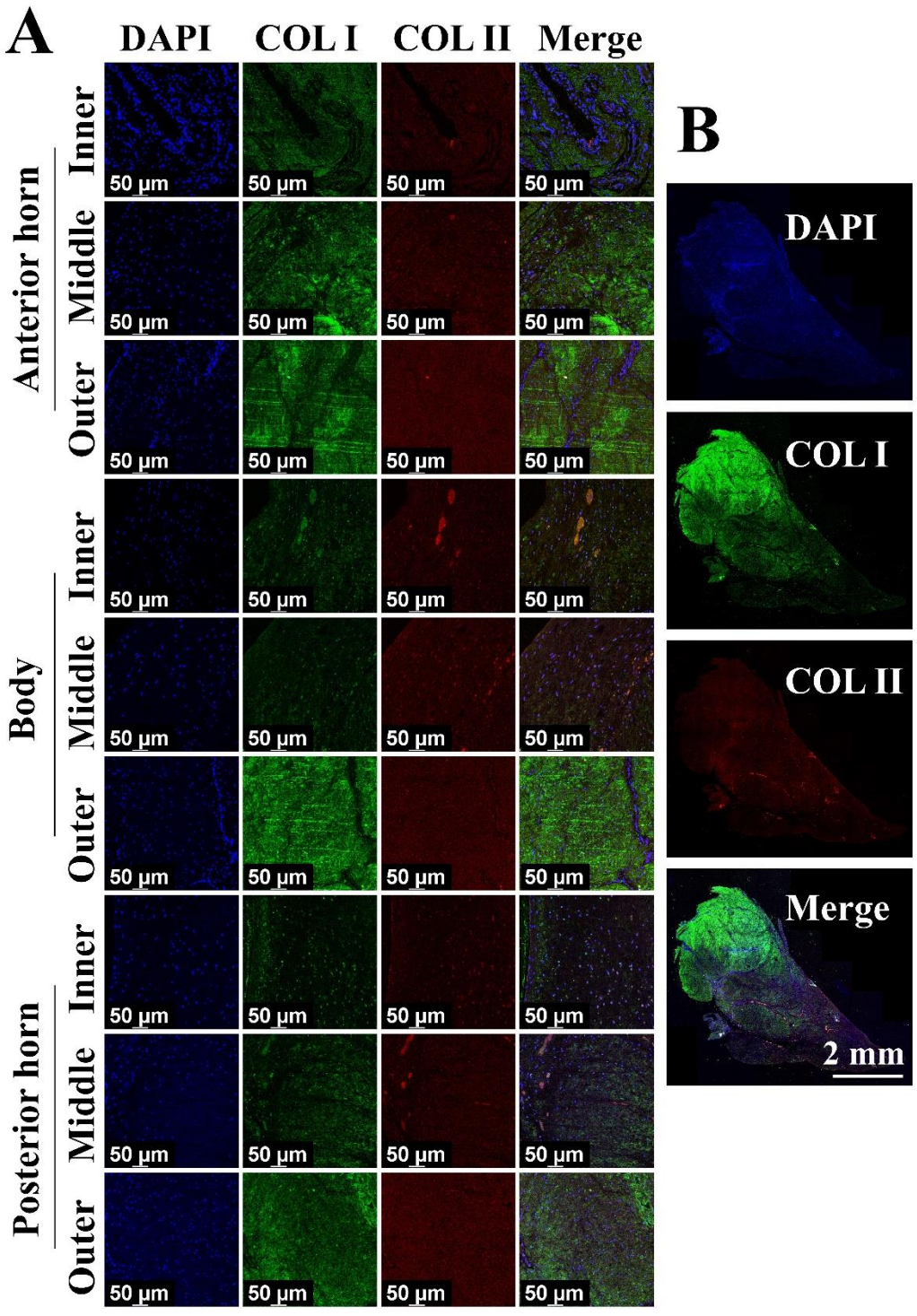
A
DAPI
COL I
COL II
Merge
Anterior horn
Inner
Middle
Outer
Body
Inner
Middle
Outer
Posterior horn
Inner
Middle
Outer
50 μm
B
DAPI
COL I
COL II
Merge
2 mm

Supplemental figure 2. The comprehensive COL I and COL II immunofluorescence in the inner, middle, outer zone of anterior horn, body and posterior horn of subtotal meniscectomy group at 2 months postoperatively. (A) the amplified image in the corresponding zone; **(B)** the general image.

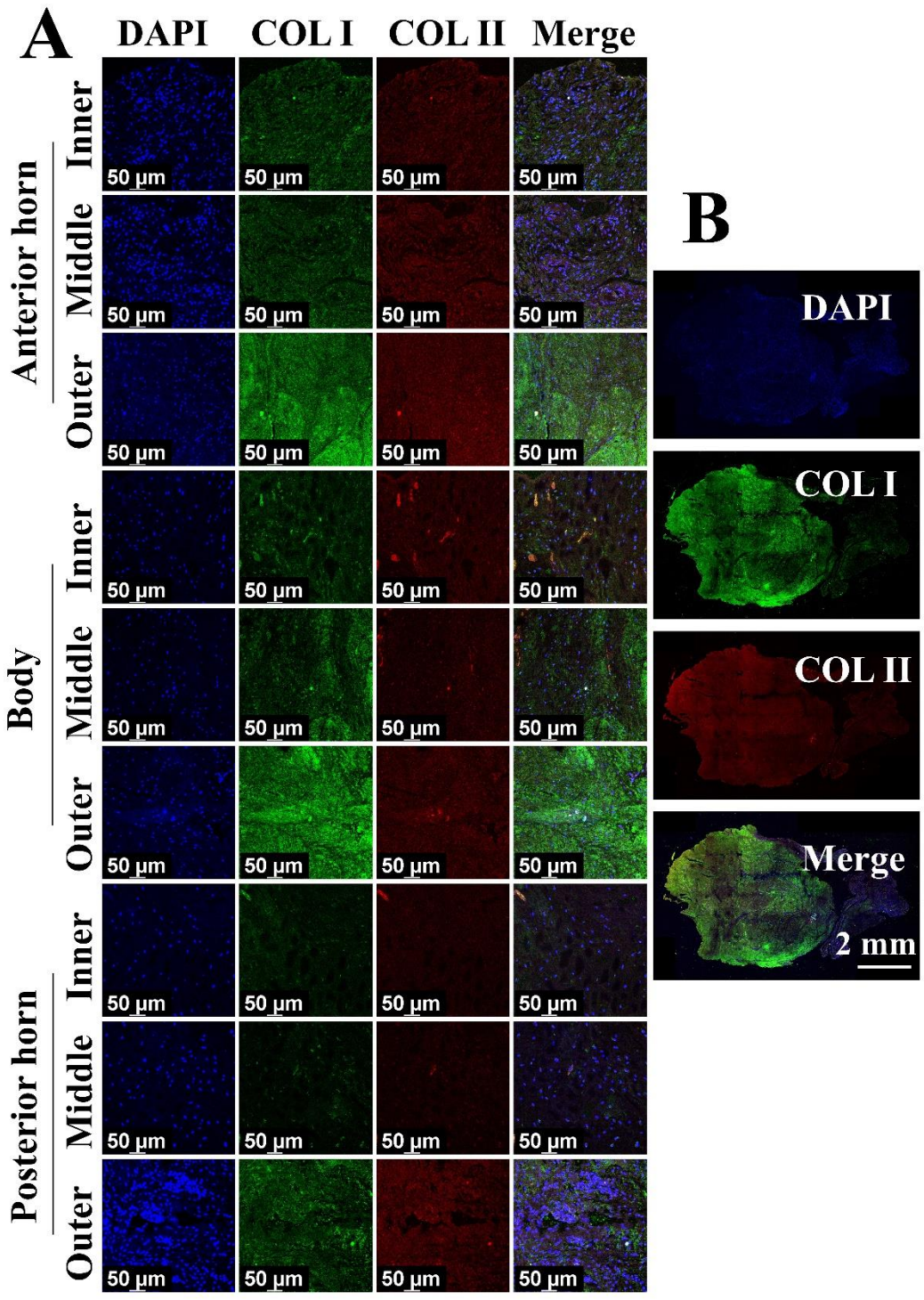
A
DAPI
COL I
COL II
Merge
Anterior horn
Body
Posterior horn
Inner
Middle
Outer
50 μm
B
DAPI
COL I
COL II
Merge
2 mm

Supplemental figure 3. The comprehensive COL I and COL II immunofluorescence in the inner, middle, outer zone of anterior horn, body and posterior horn of subtotal meniscectomy group at 4 months postoperatively. (A) the amplified image in the corresponding zone; **(B)** the general image.

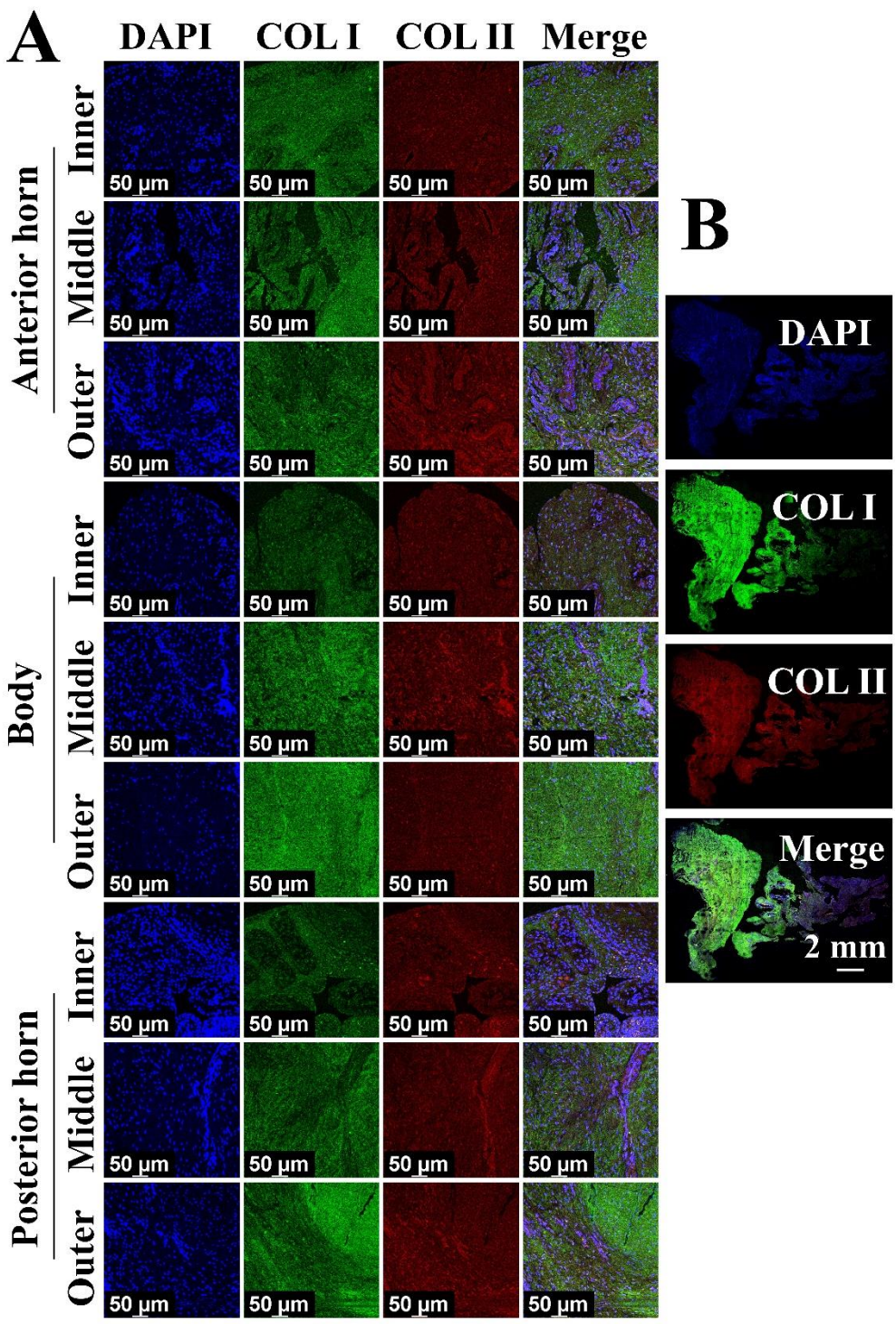
A
DAPI
COL I
COL II
Merge
Anterior horn
Inner
Middle
Outer
Body
Inner
Middle
Outer
Posterior horn
Inner
Middle
Outer
50 μm
B
DAPI
COL I
COL II
Merge
2 mm

Supplemental figure 4. The comprehensive COL I and COL II immunofluorescence in the inner, middle, outer zone of anterior horn, body and posterior horn of blank PCL scaffold group at 2 months postoperatively. (A) the amplified image in the corresponding zone; **(B)** the general image.

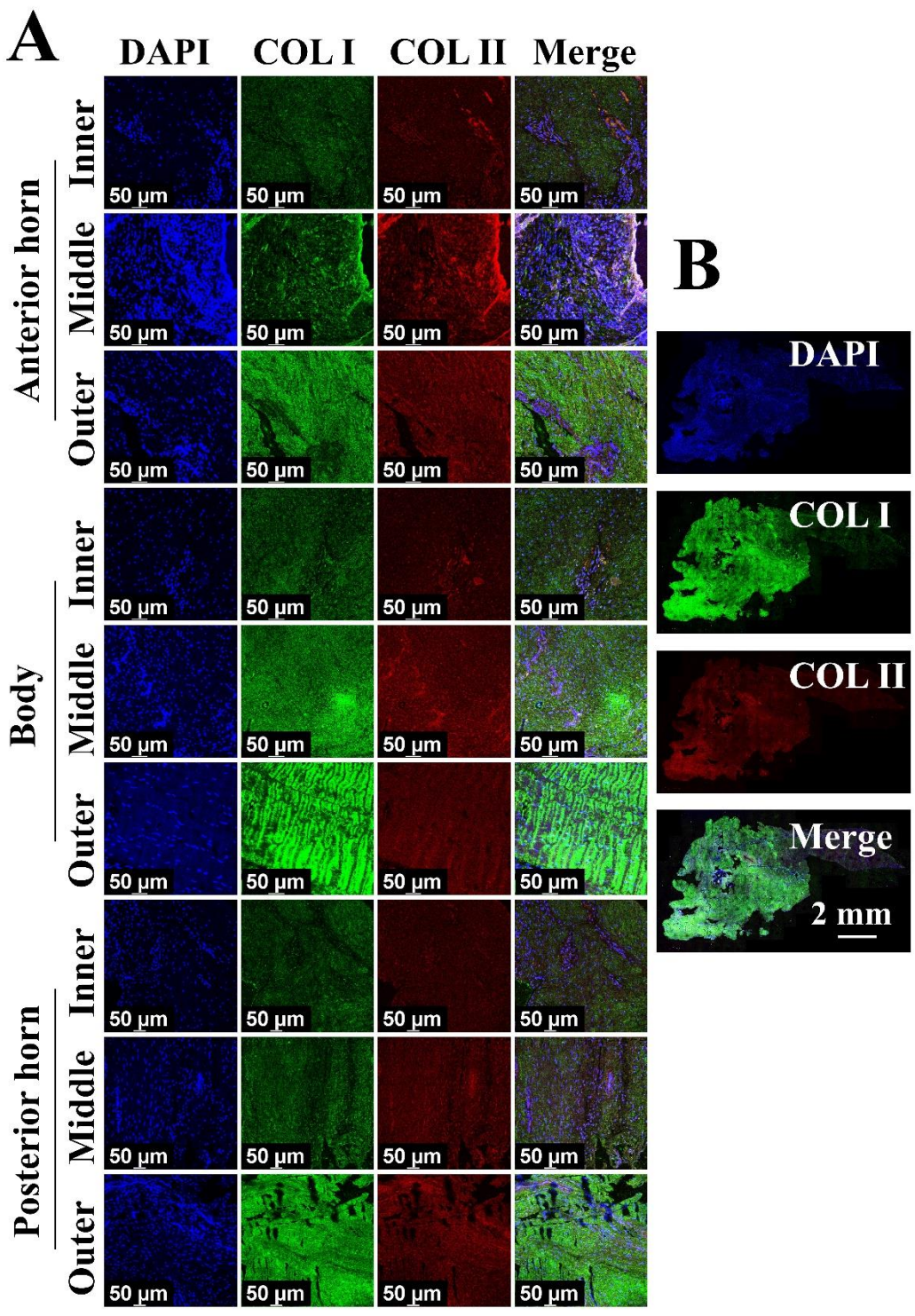
A
DAPI
COL I
COL II
Merge
Anterior horn
Inner
Middle
Outer
Body
Inner
Middle
Outer
Posterior horn
Inner
Middle
Outer
50 μm
B
DAPI
COL I
COL II
Merge
2 mm

Supplemental figure 5. The comprehensive COL I and COL II immunofluorescence in the inner, middle, outer zone of anterior horn, body and posterior horn of blank PCL scaffold group at 4 months postoperatively. (A) the amplified image in the corresponding zone; **(B)** the general image.

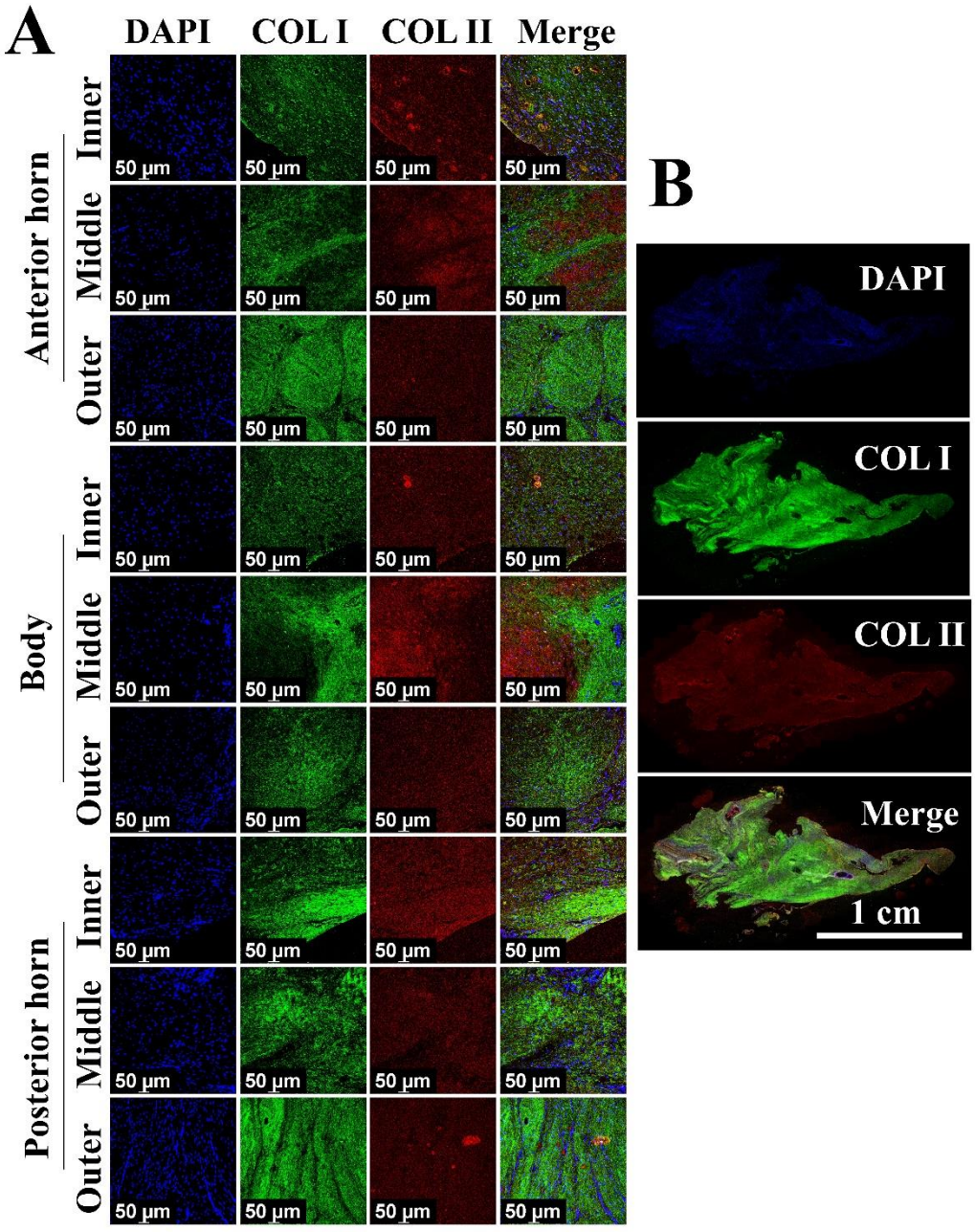
A
DAPI
COL I
COL II
Merge
Anterior horn
Body
Posterior horn
Inner
Middle
Outer
50 μm
B
DAPI
COL I
COL II
Merge
1 cm

Supplemental figure 6. The comprehensive COL I and COL II immunofluorescence in the inner, middle, outer zone of anterior horn, body and posterior horn of PCL scaffold+synovium transplant group at 2 months postoperatively. (A) the amplified image in the corresponding zone; **(B)** the general image.

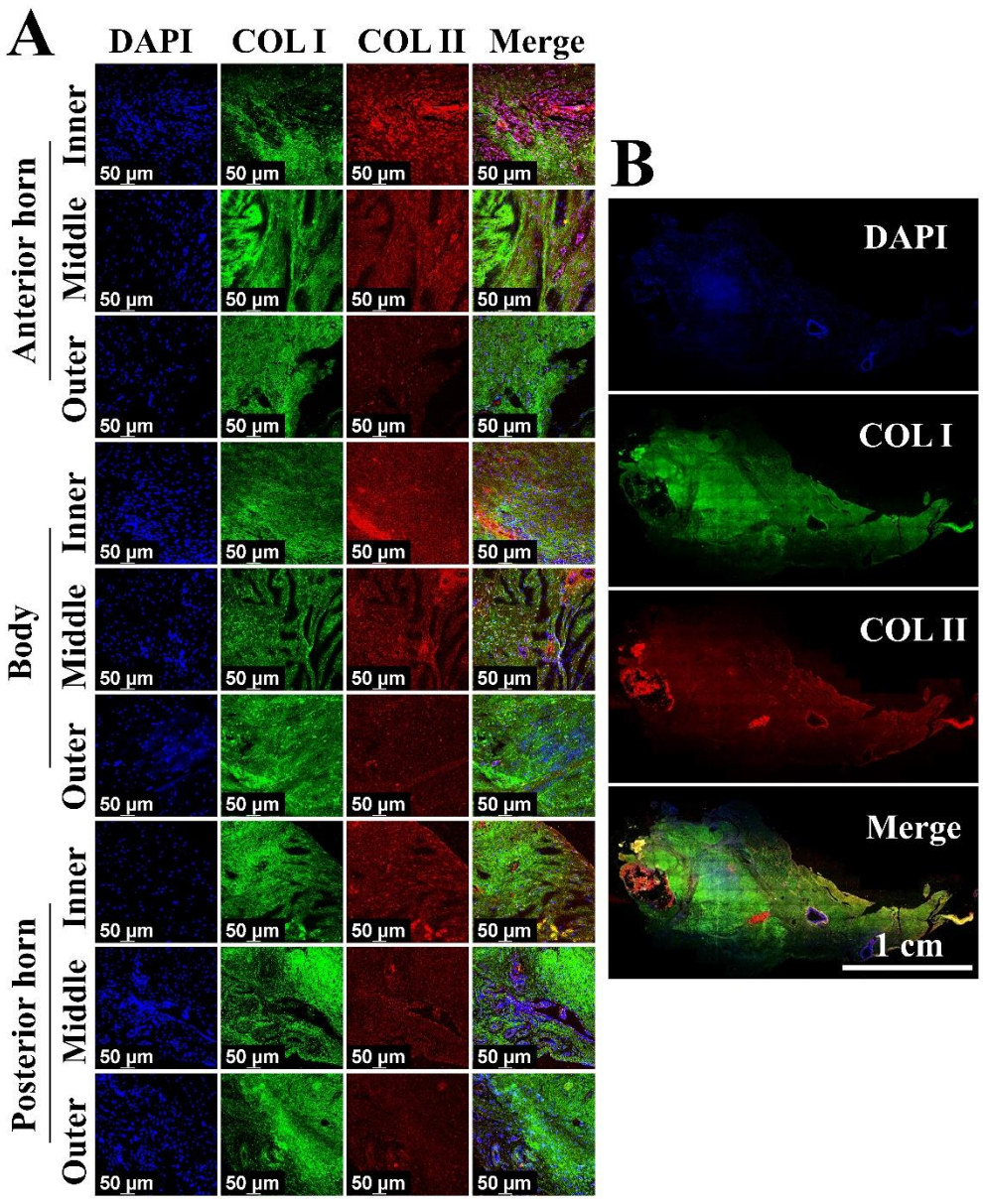
A
DAPI
COL I
COL II
Merge
Anterior horn
Body
Posterior horn
Inner
Middle
Outer
50 μm
B
DAPI
COL I
COL II
Merge
1 cm

Supplemental figure 7. The comprehensive COL I and COL II immunofluorescence in the inner, middle, outer zone of anterior horn, body and posterior horn of PCL scaffold+synovium transplant group at 4 months postoperatively. (A) the amplified image in the corresponding zone; **(B)** the general image.

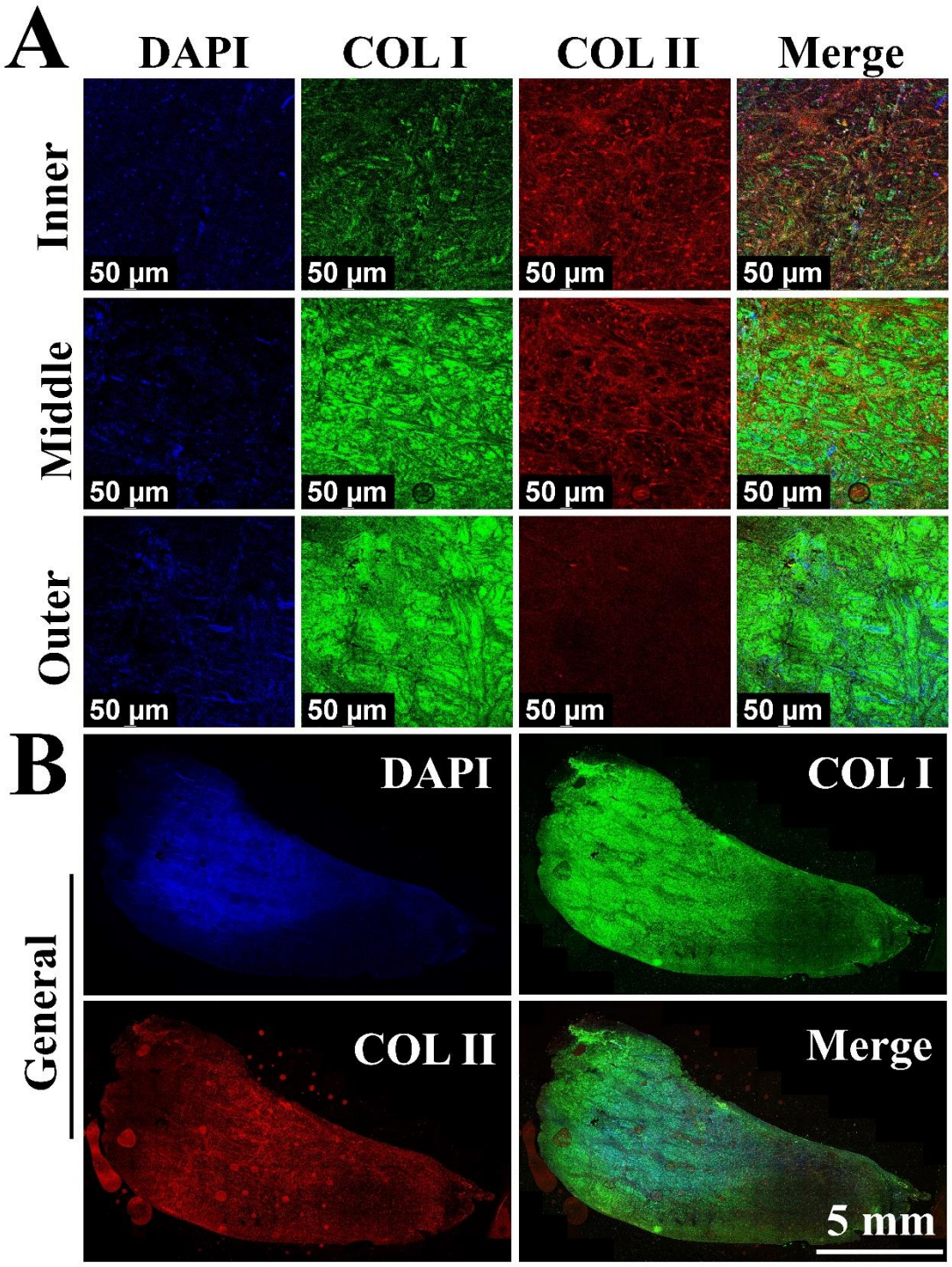
A
DAPI
COL I
COL II
Merge
Inner
Middle
Outer
50 μm
B
General
DAPI
COL I
COL II
Merge
5 mm

Supplemental figure 8. The comprehensive COL I and COL II immunofluorescence in the inner, middle, outer zone of native porcine meniscus. **(A)** the amplified image in the corresponding zone; **(B)** the general image.

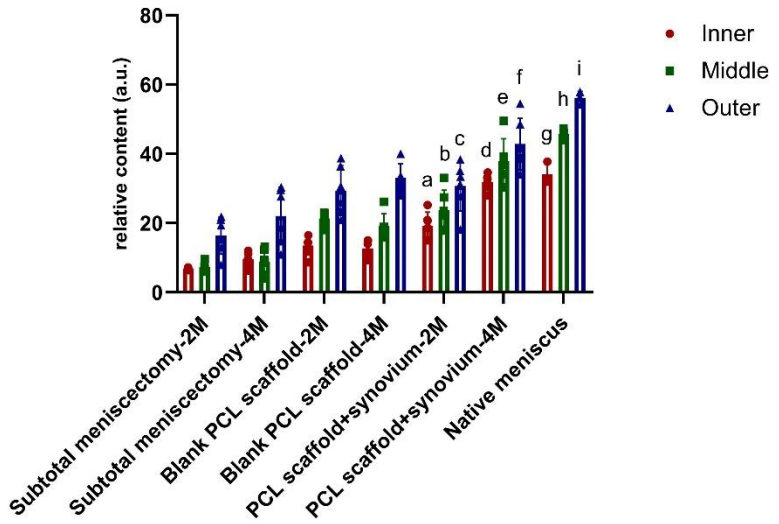
80
60
40
20
0
relative content (a.u.)
a
b
c
d
e
f
g
h
i
Inner
Middle
Outer
Subtotal meniscectomy-2M
Subtotal meniscectomy-4M
Blank PCL scaffold-2M
Blank PCL scaffold-4M
PCL scaffold+synovium-2M
PCL scaffold+synovium-4M
Native meniscus

Supplemental figure 9. The semiquantitative assessment of COL I of different groups in different regions. a: $p<0.05$ compared to inner of meniscectomy-2M, scaffold+synovium-4M, native meniscus; and outer of scaffold+synovium-2M; b: $p<0.05$ compared to middle of meniscectomy-2M, scaffold+synovium-4M, native meniscus; c: $p<0.05$ compared to outer of meniscectomy-2M, scaffold+synovium-4M, native meniscus; d: $p<0.05$ compared to inner of meniscectomy-4M, blank scaffold-4M; and outer of scaffold+synovium-4M; e: $p<0.05$ compared to middle of meniscectomy-4M, blank scaffold-4M; f: $p<0.05$ compared to outer of meniscectomy-4M, native meniscus; g: $p<0.05$ compared to inner of meniscectomy-2/4M, blank scaffold-2/4M; and outer of native meniscus; h: $p<0.05$ compared to middle of meniscectomy-2/4M, blank scaffold-2/4M; i: $p<0.05$ compared to outer of meniscectomy-2/4M, blank scaffold-2/4M; n=3 for native meniscus; n=6 for other groups; two-way ANOVA.

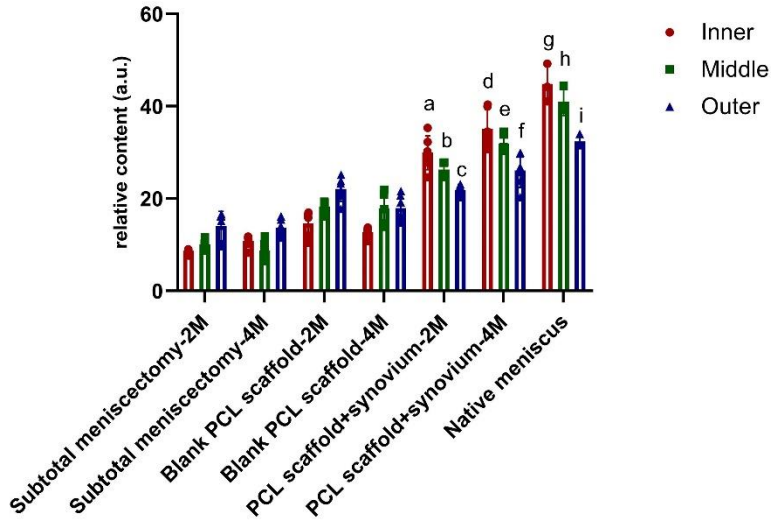
60
40
20
0
relative content (a.u.)
a
b
c
d
e
f
g
h
i
Inner
Middle
Outer
Subtotal meniscectomy-2M
Subtotal meniscectomy-4M
Blank PCL scaffold-2M
Blank PCL scaffold-4M
PCL scaffold+synovium-2M
PCL scaffold+synovium-4M
Native meniscus

Supplemental figure 10. The semiquantitative assessment of COL II of different groups in different regions. a: $p<0.05$ compared to inner of meniscectomy-2M, blank scaffold-2M, native meniscus; and outer of scaffold+synovium-2M; b: $p<0.05$ compared to middle of meniscectomy-2M, blank scaffold-2M, scaffold+synovium-4M, native meniscus; c: $p<0.05$ compared to outer of meniscectomy-2M, native meniscus; d: $p<0.05$ compared to inner of meniscectomy-4M, blank scaffold-4M, native meniscus; and outer of scaffold+synovium-4M; e: $p<0.05$ compared to middle of meniscectomy-4M, blank scaffold-4M, native meniscus; and outer of scaffold+synovium-4M; f: $p<0.05$ compared to outer of meniscectomy-4M, blank scaffold-4M; g: $p<0.05$ compared to inner of meniscectomy-2/4M, blank scaffold-2/4M; and outer of native meniscus; h: $p<0.05$ compared to middle of meniscectomy-2/4M, blank scaffold-2/4M; and outer of native meniscus; i: $p<0.05$ compared to outer of meniscectomy-2/4M, blank scaffold-2/4M; n=3 for native meniscus; n=6 for other groups; two-way ANOVA.

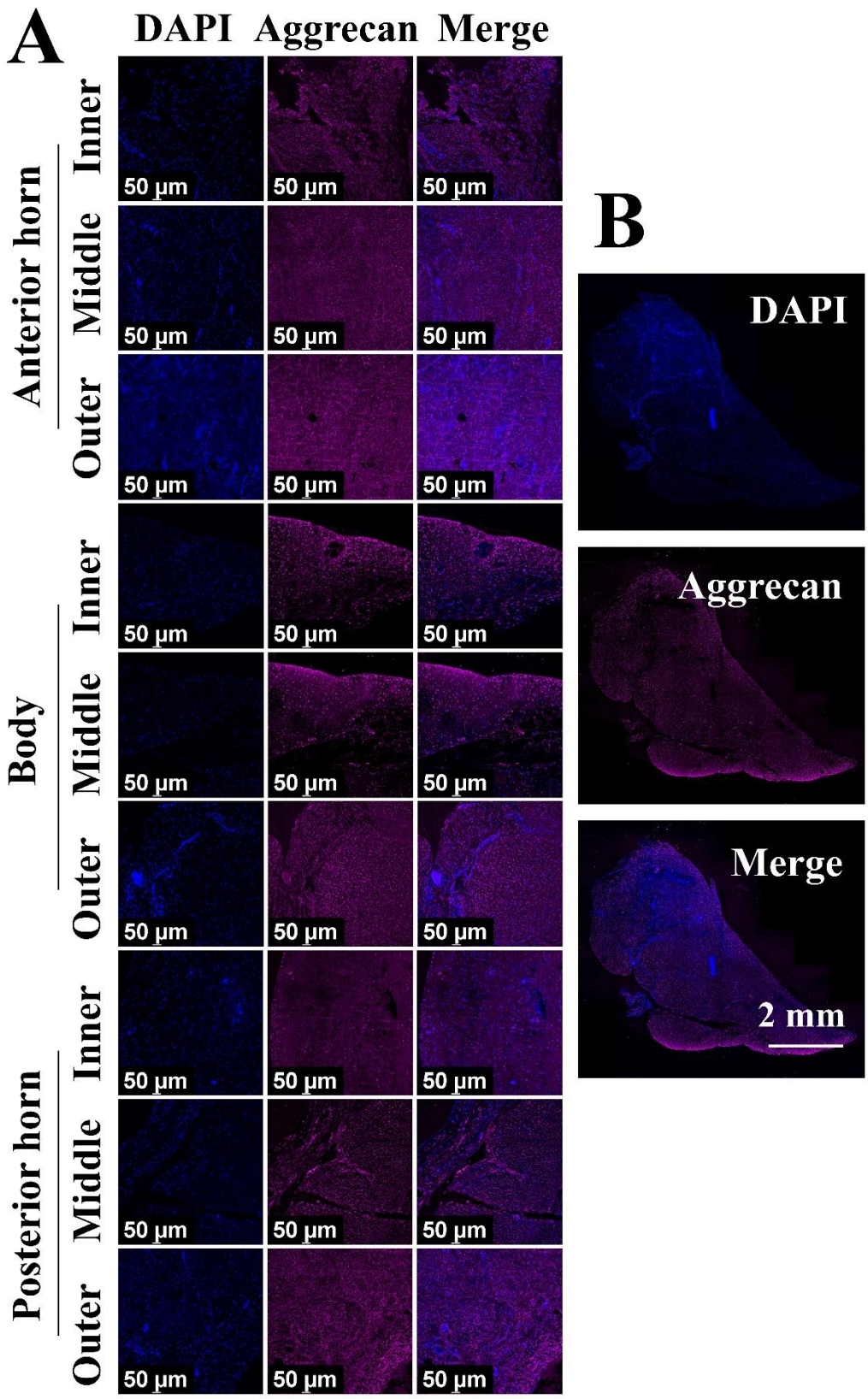
A
DAPI
Aggrecan
Merge
Anterior horn
Inner
Middle
Outer
Body
Inner
Middle
Outer
Posterior horn
Inner
Middle
Outer
50 μm
B
DAPI
Aggrecan
Merge
2 mm

Supplemental figure 11. The comprehensive aggrecan immunofluorescence in the inner, middle, outer zone of anterior horn, body and posterior horn of subtotal meniscectomy group at 2 months postoperatively. (A) the amplified image in the corresponding zone; **(B)** the general image.

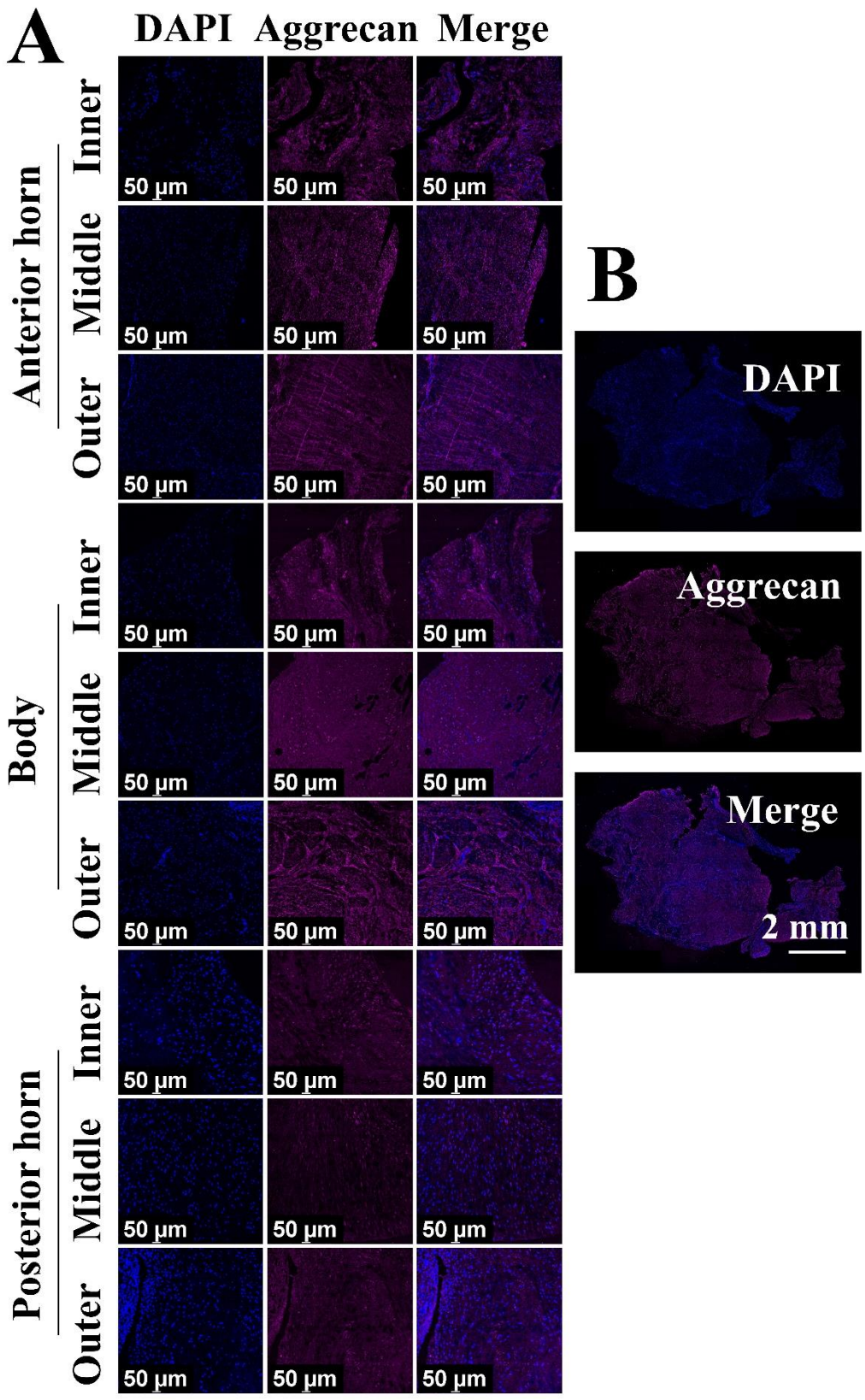
A
DAPI
Aggrecan
Merge
Anterior horn
Inner
Middle
Outer
Body
Inner
Middle
Outer
Posterior horn
Inner
Middle
Outer
50 μm
B
DAPI
Aggrecan
Merge
2 mm

Supplemental figure 12. The comprehensive aggrecan immunofluorescence in the inner, middle, outer zone of anterior horn, body and posterior horn of subtotal meniscectomy group at 4 months postoperatively. (A) the amplified image in the corresponding zone; **(B)** the general image.

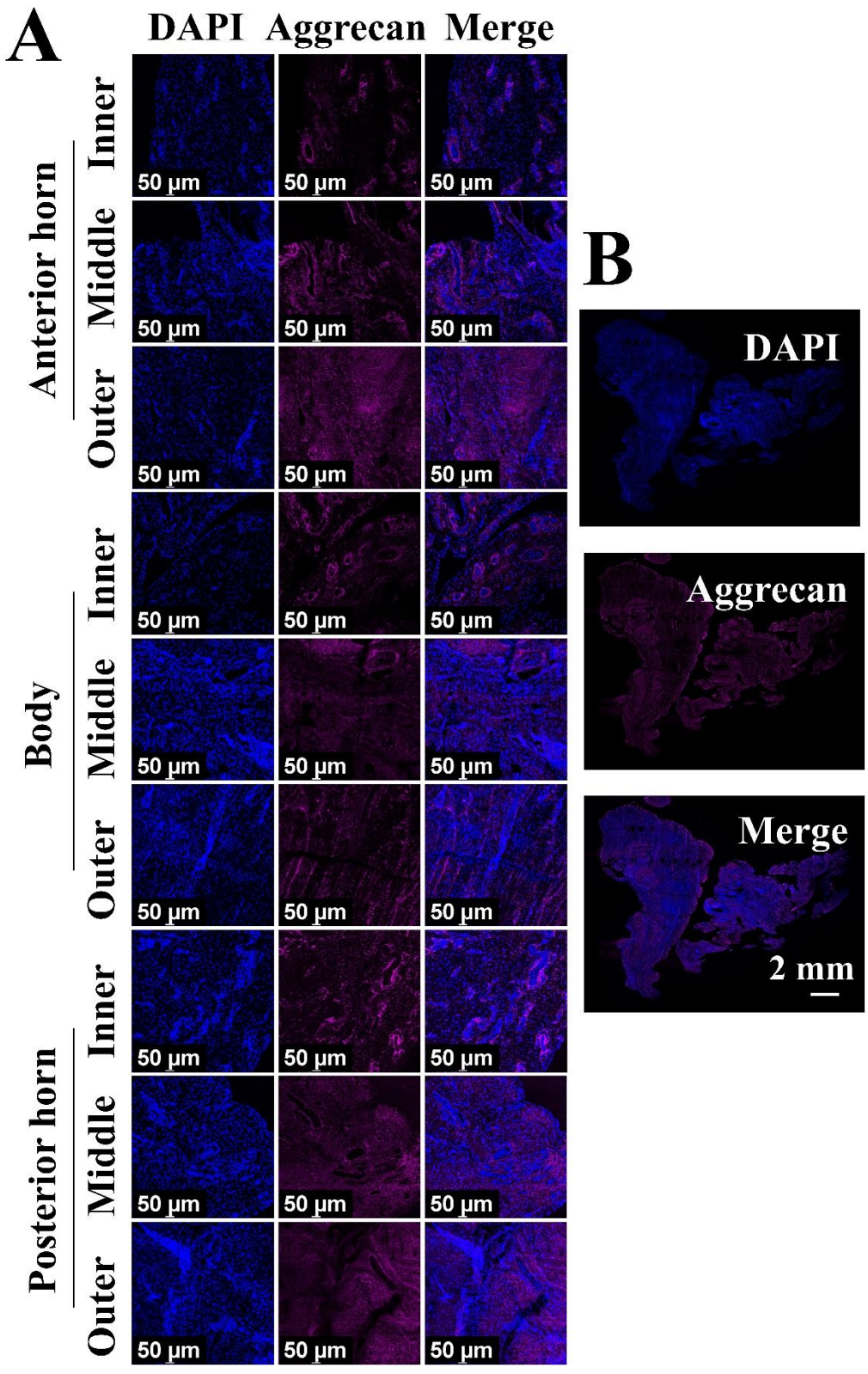
A
DAPI
Aggrecan
Merge
Anterior horn
Inner
Middle
Outer
Body
Inner
Middle
Outer
Posterior horn
Inner
Middle
Outer
50 μm
B
DAPI
Aggrecan
Merge
2 mm

Supplemental figure 13. The comprehensive aggrecan immunofluorescence in the inner, middle, outer zone of anterior horn, body and posterior horn of blank PCL scaffold group at 2 months postoperatively. (A) the amplified image in the corresponding zone; **(B)** the general image.

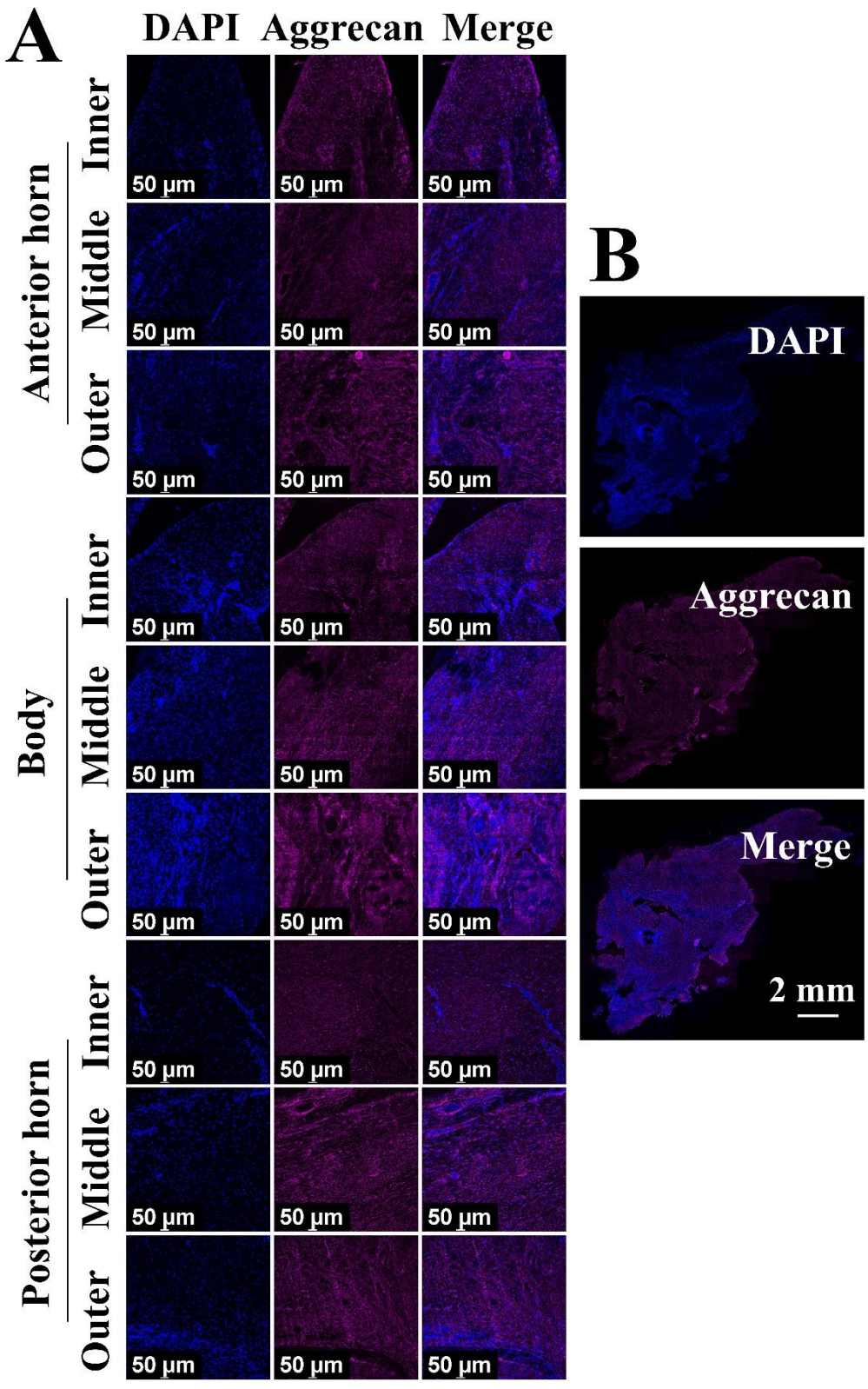
A
DAPI
Aggrecan
Merge
Anterior horn
Inner
Middle
Outer
Body
Inner
Middle
Outer
Posterior horn
Inner
Middle
Outer
50 μm
B
DAPI
Aggrecan
Merge
2 mm

Supplemental figure 14. The comprehensive aggrecan immunofluorescence in the inner, middle, outer zone of anterior horn, body and posterior horn of blank PCL scaffold group at 4 months postoperatively. (A) the amplified image in the corresponding zone; **(B)** the general image.

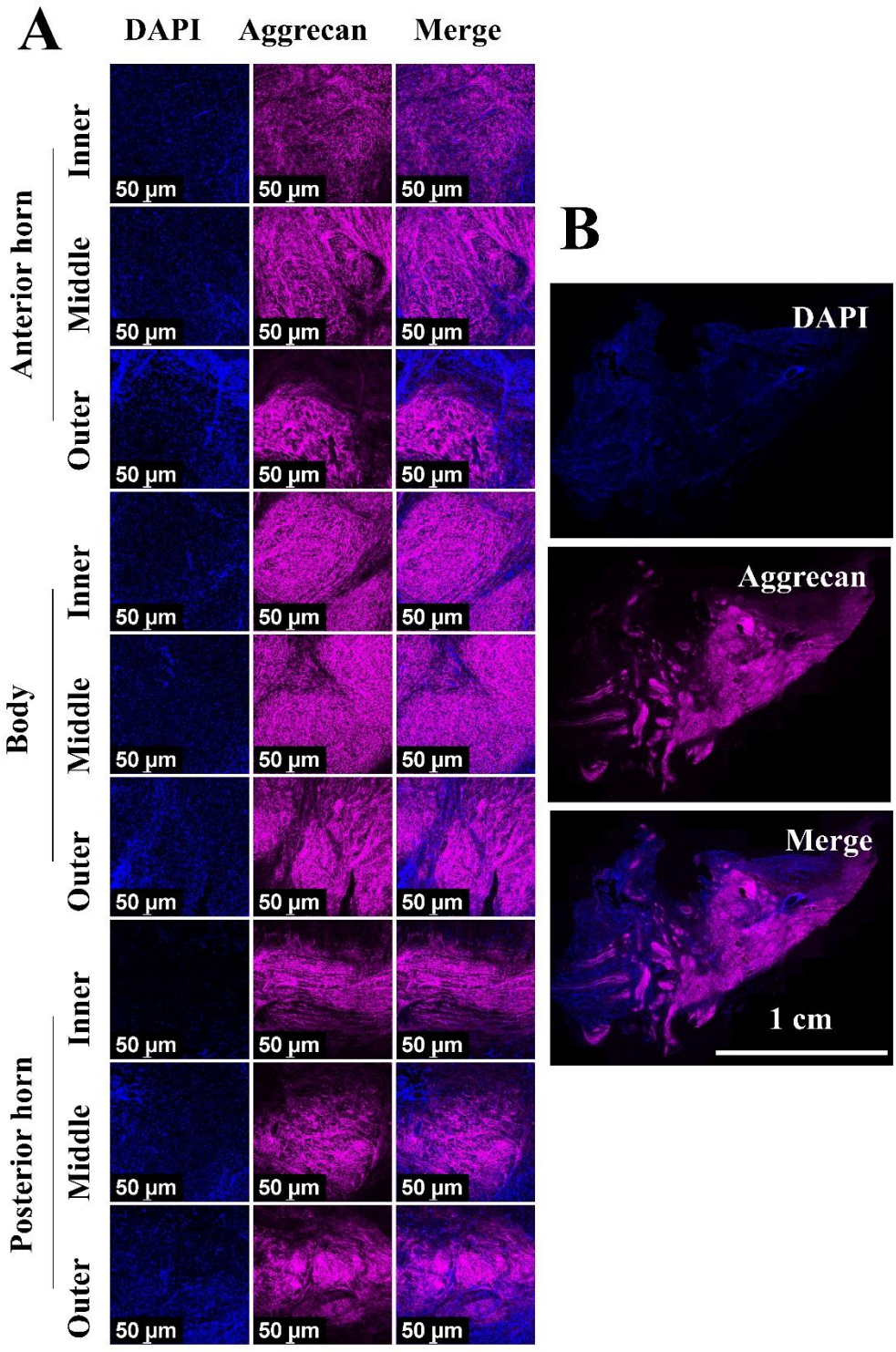
A
DAPI
Aggrecan
Merge
Anterior horn
Body
Posterior horn
Inner
Middle
Outer
50 μm
B
DAPI
Aggrecan
Merge
1 cm

Supplemental figure 15. The comprehensive aggrecan immunofluorescence in the inner, middle, outer zone of anterior horn, body and posterior horn of PCL scaffold+synovium transplant group at 2 months postoperatively. (A) the amplified image in the corresponding zone; **(B)** the general image.

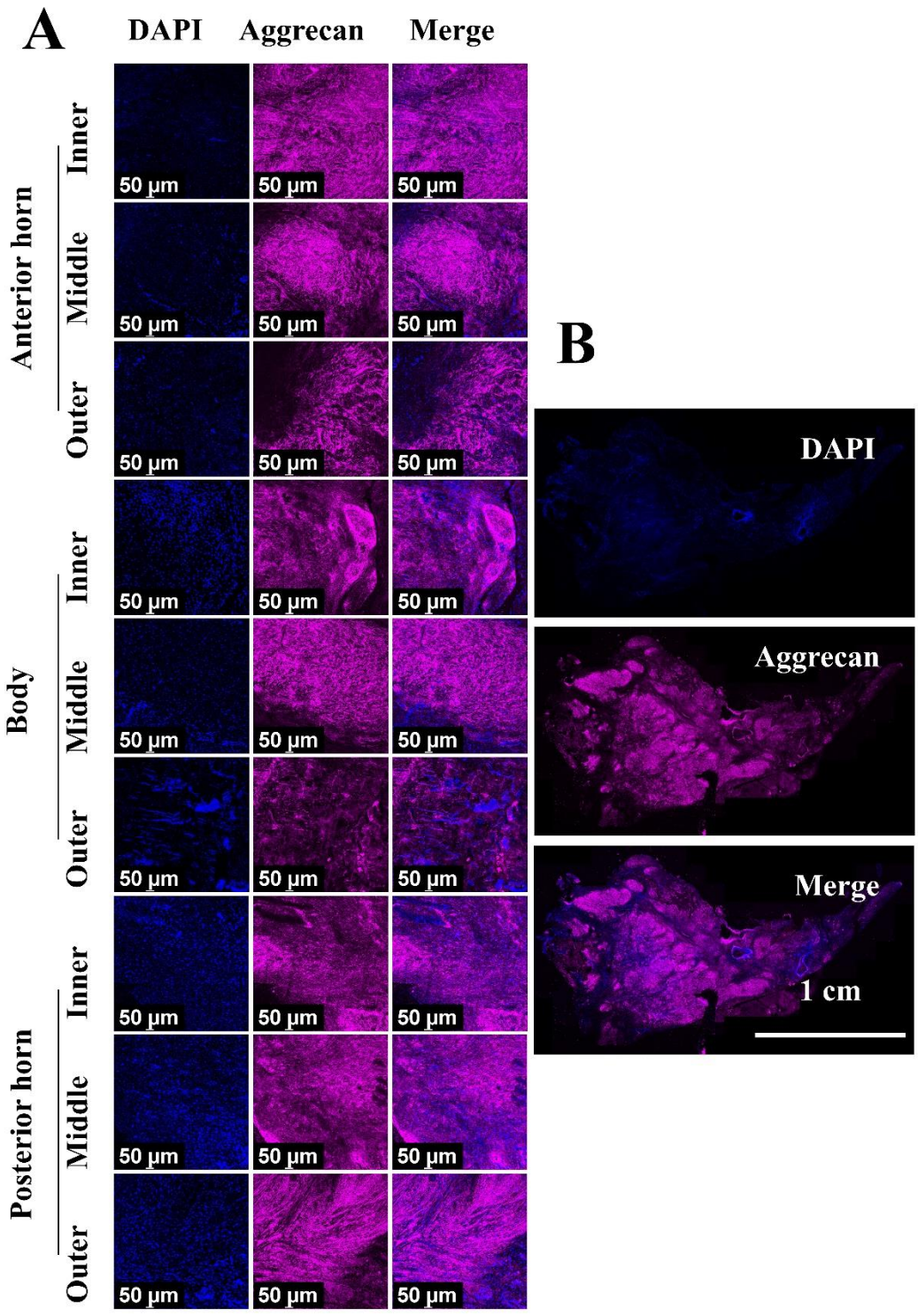
A
DAPI
Aggrecan
Merge
Anterior horn
Body
Posterior horn
Inner
Middle
Outer
50 μm
B
DAPI
Aggrecan
Merge
1 cm

Supplemental figure 16. The comprehensive aggrecan immunofluorescence in the inner, middle, outer zone of anterior horn, body and posterior horn of PCL scaffold+synovium transplant group at 4 months postoperatively. (A) the amplified image in the corresponding zone; **(B)** the general image.

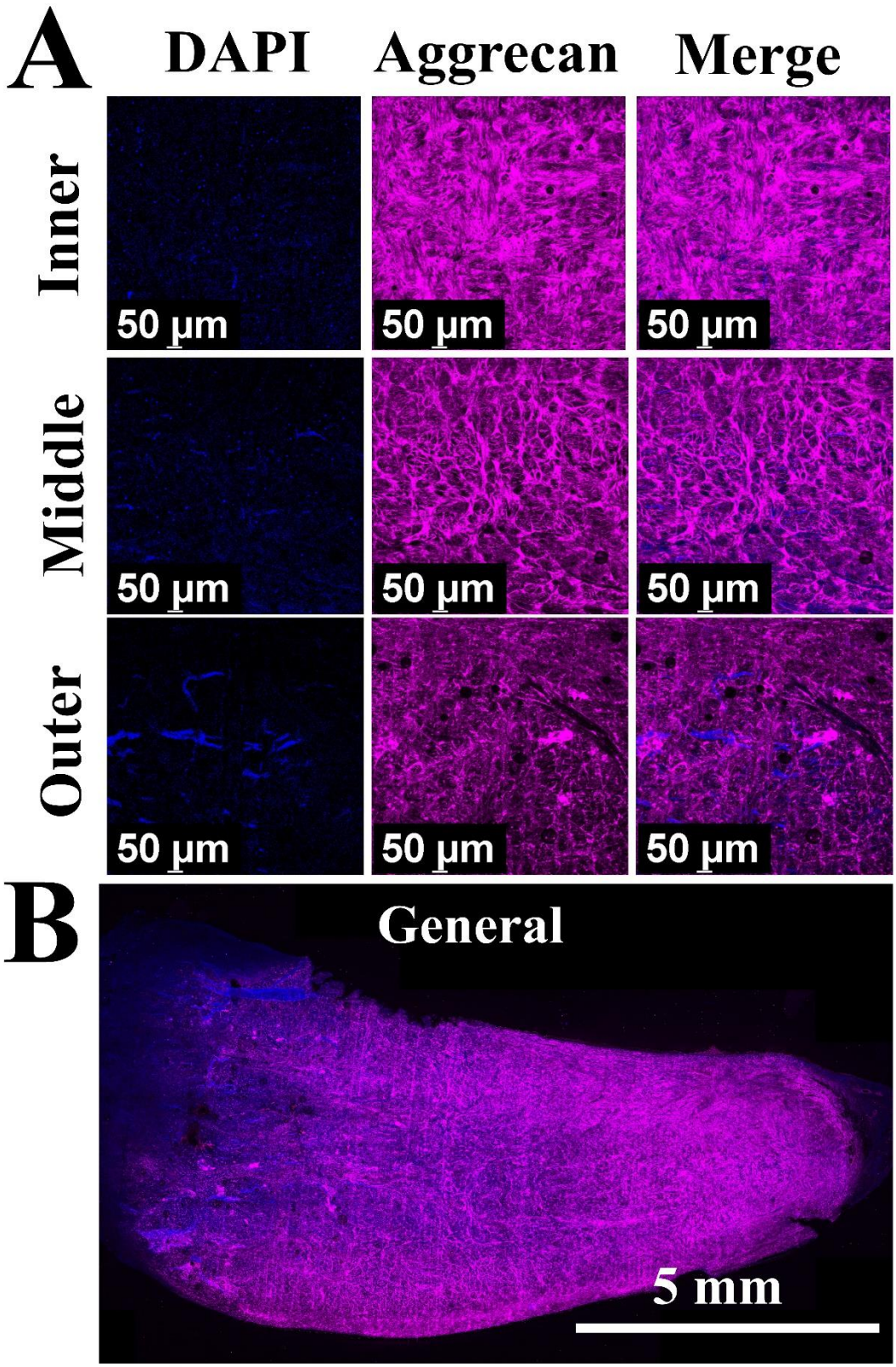
A
DAPI
Aggrecan
Merge
Inner
Middle
Outer
50 μm
B
General
5 mm

Supplemental figure 17. The comprehensive aggrecan immunofluorescence in the inner, middle, outer zone of native porcine meniscus. (A) the amplified image in the corresponding zone; **(B)** the general image.

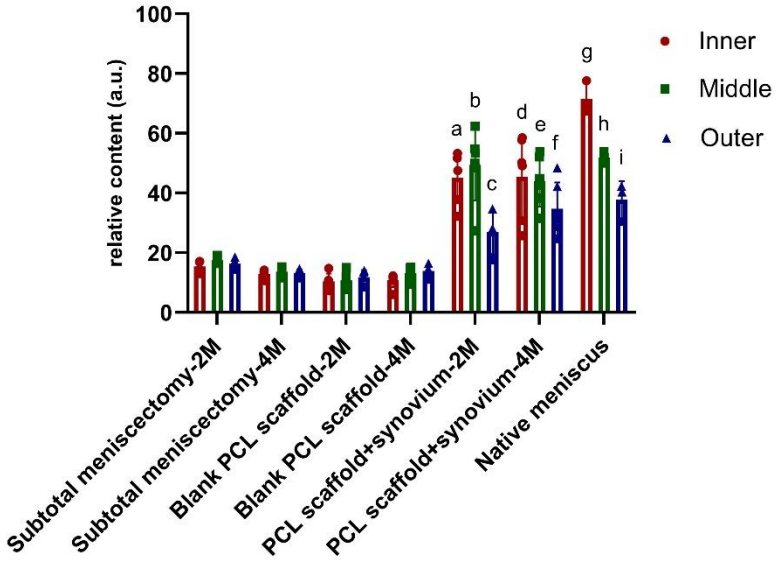
relative content (a.u.)
100
80
60
40
20
0
a
b
c
d
e
f
g
h
i
Inner
Middle
Outer
Subtotal meniscectomy-2M
Subtotal meniscectomy-4M
Blank PCL scaffold-2M
Blank PCL scaffold-4M
PCL scaffold+synovium-2M
PCL scaffold+synovium-4M
Native meniscus

Supplemental figure 18. The semiquantitative assessment of aggrecan of different groups in different regions. a: $p<0.05$ compared to inner of meniscectomy-2M, blank scaffold-2M, native meniscus and outer of scaffold+synovium-2M; b: $p<0.05$ compared to middle of meniscectomy-2M, blank scaffold-2M; c: $p<0.05$ compared to outer of blank scaffold-2M; d: $p<0.05$ compared to inner of meniscectomy-4M, blank scaffold-4M, native meniscus; e: $p<0.05$ compared to middle of meniscectomy-4M, blank scaffold-4M; f: $p<0.05$ compared to outer of meniscectomy-4M, blank scaffold-4M; g: $p<0.05$ compared to inner of other groups; h: $p<0.05$ compared to middle of meniscectomy-2/4M, blank scaffold-2/4M, and inner of native meniscus; i: $p<0.05$ compared to outer of meniscectomy-2/4M, blank scaffold-2/4M, and inner of native meniscus; n=3 for native meniscus; n=6 for other groups; two-way ANOVA.

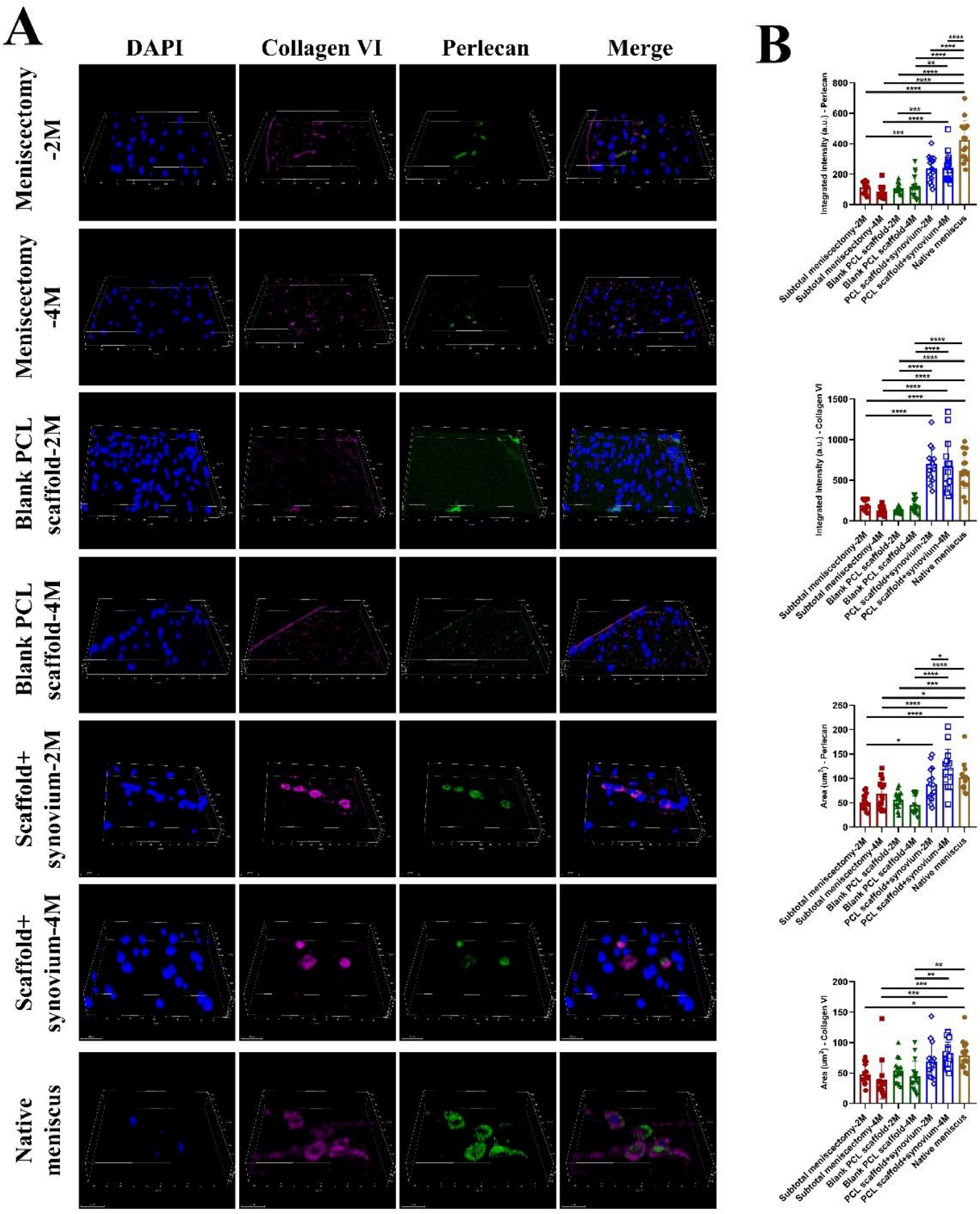
A
DAPI
Collagen VI
Perlecan
Merge
Meniscectomy -2M
Meniscectomy -4M
Blank PCL scaffold-2M
Blank PCL scaffold-4M
Scaffold+ synovium-2M
Scaffold+ synovium-4M
Native meniscus
B
Integrated intensity (a.u.) - Perlecan
Integrated intensity (a.u.) - Collagen VI
Area (um²) - Perlecan
Area (um²) - Collagen VI
Subtotal meniscectomy-2M
Subtotal meniscectomy-4M
Blank PCL scaffold-2M
Blank PCL scaffold-4M
PCL scaffold+synovium-2M
PCL scaffold+synovium-4M
Native meniscus

Supplemental figure 19. The 3D image and semiquantitative analysis of perlecan and collagen VI. (A) the 3D image of perlecan and collagen VI immunofluorescence; **(B)** the semiquantitative analysis of integrated intensity and area of perlecan and collagen VI in different groups; n=15, one-way ANOVA.

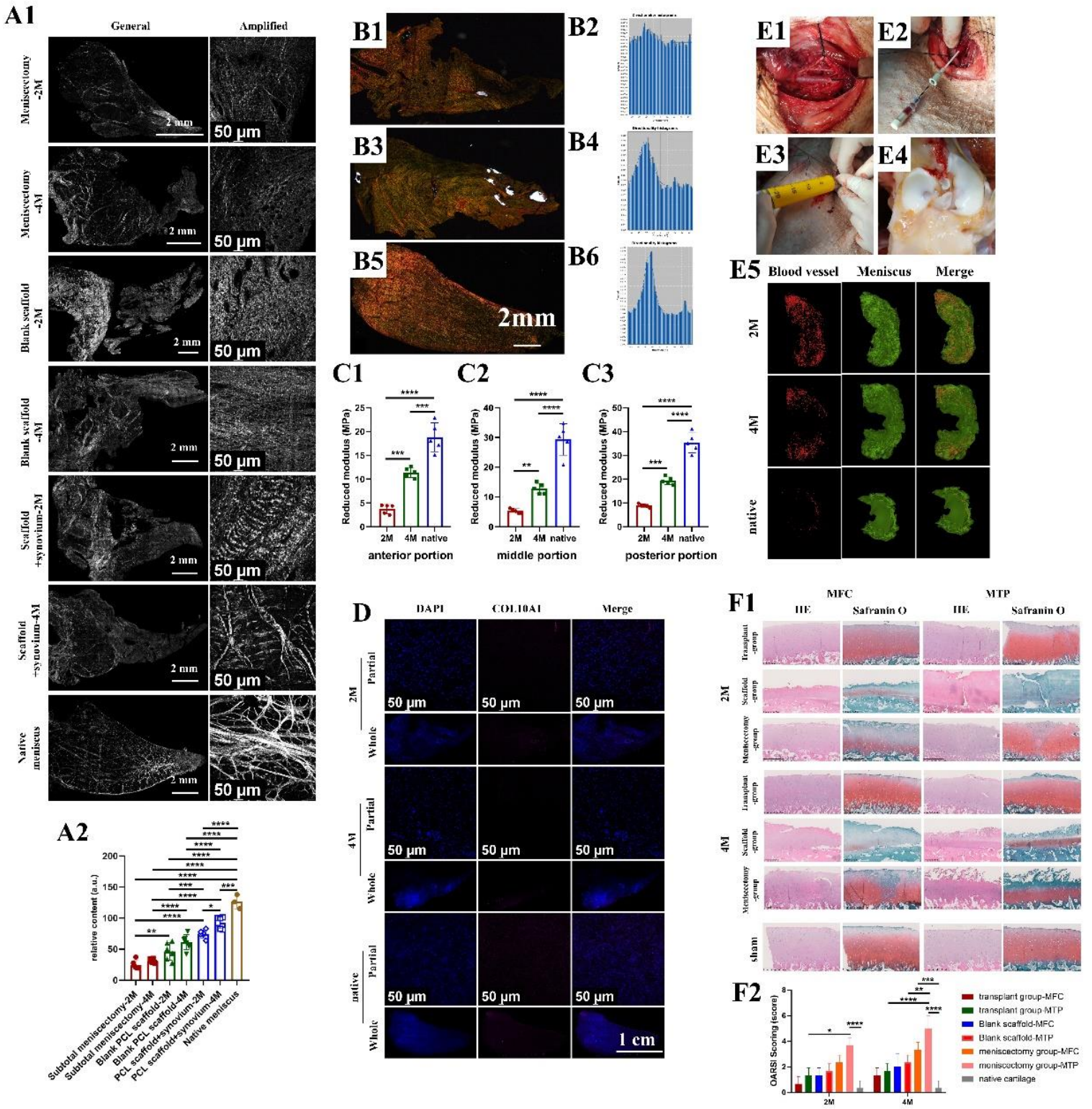
A1
General
Amplified
Meniscectomy -2M
Meniscectomy -4M
Blank scaffold -2M
Blank scaffold -4M
Scaffold +synovium-2M
Scaffold +synovium-4M
Native meniscus
2 mm
50 μm
A2
relative content (a.u.)
Subtotal meniscectomy-2M
Subtotal meniscectomy-4M
Blank PCL scaffold-2M
Blank PCL scaffold-4M
PCL scaffold+synovium-2M
PCL scaffold+synovium-4M
Native meniscus
B1
B2
B3
B4
B5
B6
2mm
C1
C2
C3
Reduced modulus (MPa)
2M
4M
native
anterior portion
middle portion
posterior portion
D
DAPI
COL10A1
Merge
2M
4M
native
Partial
Whole
50 μm
1 cm
E1
E2
E3
E4
E5
Blood vessel
Meniscus
Merge
2M
4M
native
F1
MFC
MTP
HE
Safranin O
Transplant group
Scaffold group
Meniscectomy group
sham
F2
OARSI Scoring (score)
transplant group-MFC
transplant group-MTP
Blank scaffold-MFC
Blank scaffold-MTP
meniscectomy group-MFC
meniscectomy group-MTP
native cartilage

Supplemental figure 20. The characterization of collagens, mechanical properties, hypertrophy in regenerated tissue. The angiography of blood vessels in regenerated tissue. The histological analyses of joint cartilage degeneration. (A) The characterization of collagen within regenerated tissue using two-photon microscopy (**A1,** the representative images; **A2,** the semiquantitative analysis of collagen content, n=3 for native meniscus, n=6 for other groups, one-way ANOVA). **(B)** The assessment of collagen fiber arrangement of regenerated tissue in PCL scaffold+synovium transplant group and native meniscus using Sirius red staining (**B1,** the representative image of PCL scaffold+synovium transplant group-2M; **B2,** the histogram of collagen directionality; **B3,** the representative image of PCL scaffold+synovium transplant group-4M; **B4,** the histogram of collagen directionality; **B5,** representative image of native menisci; **B6,** the histogram of collagen directionality of native menisci). **(C)** The reduced modulus of regenerated tissue and native menisci in anterior, middle and posterior portion (**C1**, anterior portion; **C2,** middle portion; **C3,** posterior portion; n=5, one-way ANOVA). **(D)** The assessment of COL10A1 expression in regenerated tissue and native menisci. **(E)** The angiography of regenerated tissue and native menisci (**E1,** the separation of femoral artery; **E2,** the puncture of femoral artery; **E3,** the injection of angiographic contrast agent; **E4,** the representative macroscopic image of native porcine knee after angiography; **E5,** the 3D model of blood vessels in regenerated tissue and native porcine menisci). **(F)** The histological assessment of cartilage degeneration (**F1,** HE and safranin O staining of cartilage tissue; Transplant-group represents PCL scaffold+synovium transplant group; Scaffold group represents

blank PCL scaffold group; Meniscectomy group represents subtotal meniscectomy group; **F2,** the OARSI scoring of knee cartilage degeneration; n=3, two-way ANOVA).

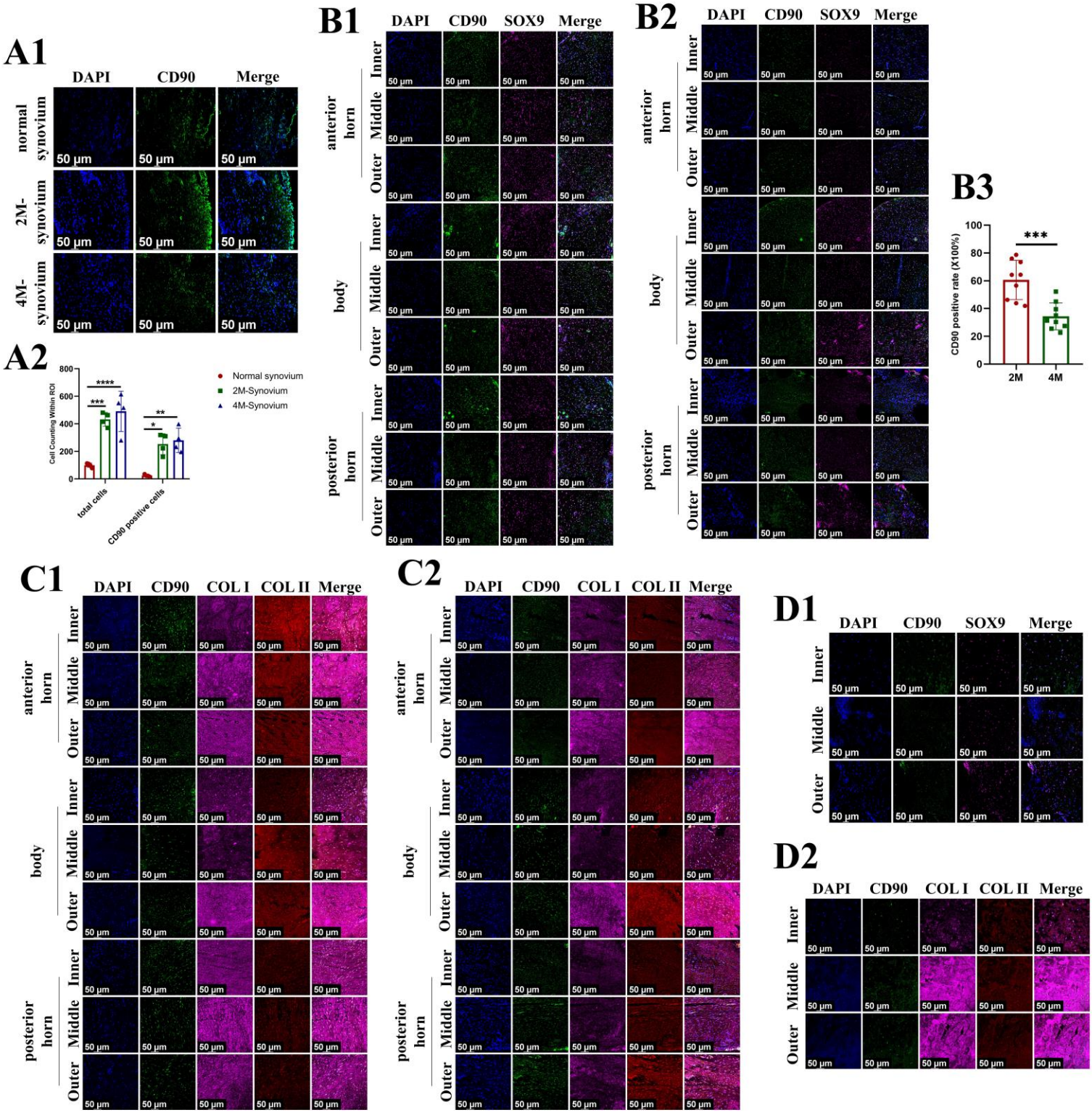
A1
DAPI
CD90
Merge
normal synovium
2M-synovium
4M-synovium
50 μm
A2
Cell Counting Within ROI
800
600
400
200
0
****
***
**
*
total cells
CD90 positive cells
Normal synovium
2M-Synovium
4M-Synovium
B1
DAPI
CD90
SOX9
Merge
anterior horn
body
posterior horn
Inner
Middle
Outer
B2
B3
CD90 positive rate (X100%)
100
80
60
40
20
0
***
2M
4M
C1
DAPI
CD90
COL I
COL II
Merge
C2
D1
D2

Supplemental figure 21. The MSCs within synovium transplant differentiate into fibrochondrocytes. (a) The identification of MSCs in synovium of normal and postoperative porcine knee joint (**a1,** identification of MSCs expressing CD90 in synovium; **a2,** the counting of total cells and CD90 positive cells in synovium, n=4, one-way ANOVA). **(b)** The immunofluorescent co-staining of CD90 and SOX9 in regenerated tissue (**b1,** regenerated tissue at 2 months postoperatively; **b2,** regenerated tissue at 4 months postoperatively; **b3,** the rate of CD90 positive cells within regenerated tissue, n=9, unpaired *t*-test). **(c)** The immunofluorescent co-staining of CD90, COL I, COL II in regenerated tissue (**c1,** 2 months postoperatively; **c2,** 4 months postoperatively). **(d)** The immunofluorescent assessment of MSCs in native porcine menisci (**d1,** the immunofluorescent co-staining of CD90 and SOX9; **d2,** the immunofluorescent co-staining of CD90, COL I, COL II).

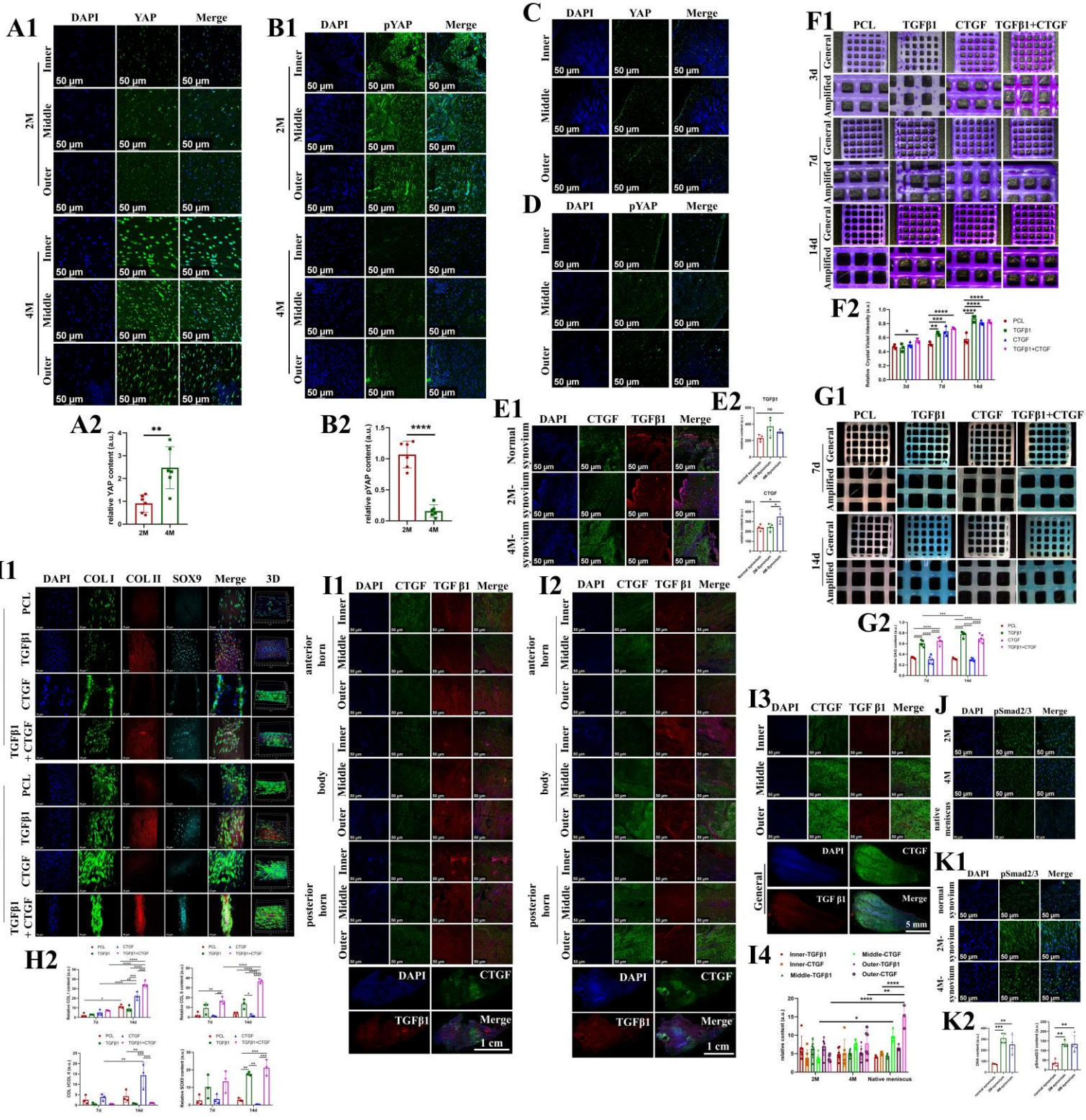
A1
DAPI
YAP
Merge
2M
4M
Inner
Middle
Outer
50 μm
B1
DAPI
pYAP
Merge
C
DAPI
YAP
Merge
D
DAPI
pYAP
Merge
A2
relative YAP content (a.u.)
2M
4M
B2
relative pYAP content (a.u.)
2M
4M
E1
DAPI
CTGF
TGFβ1
Merge
Normal synovium
2M-synovium
4M-synovium
E2
TGFβ1
CTGF
F1
PCL
TGFβ1
CTGF
TGFβ1+CTGF
3d
7d
14d
General
Amplified
F2
Relative Crystal Violet Intensity (a.u.)
PCL
TGFβ1
CTGF
TGFβ1+CTGF
G1
PCL
TGFβ1
CTGF
TGFβ1+CTGF
7d
14d
General
Amplified
G2
H1
DAPI
COL I
COL II
SOX9
Merge
3D
PCL
TGFβ1
CTGF
TGFβ1 +CTGF
7d
14d
H2
I1
DAPI
CTGF
TGF β1
Merge
anterior horn
body
posterior horn
Inner
Middle
Outer
1 cm
I2
I3
J
DAPI
pSmad2/3
Merge
native meniscus
General
5 mm
K1
normal synovium
2M-synovium
4M-synovium
I4
Inner-TGFβ1
Inner-CTGF
Middle-TGFβ1
Middle-CTGF
Outer-TGFβ1
Outer-CTGF
relative content (a.u.)
2M
4M
Native meniscus
K2

Supplemental figure 22. The expression of YAP, pYAP, TGFβ1, CTGF in regenerated tissue and native porcine menisci. The fibrochondrogenic effect of TGFβ1, CTGF on human MSCs. (A) The immunofluorescent assessment of YAP in regenerated tissue (**A1,** tissue immunofluorescence; **A2,** semiquantitative analysis of YAP, n=6, unpaired *t*-test). **(B)** The immunofluorescent assessment of pYAP in regenerated tissue (**B1,** tissue immunofluorescence; **B2,** semiquantitative analysis of pYAP, n=6, unpaired *t*-test). **(C)** The immunofluorescent assessment of YAP in native porcine menisci. **(D)** The immunofluorescent assessment of pYAP in native porcine menisci. **(E)** The immunofluorescent assessment of TGFβ1, CTGF in synovium (**E1,** tissue immunofluorescence; **E2,** semiquantitative analysis, n=4, one-way ANOVA). **(F)** The proliferation of human synovium-derived MSCs seeded onto PCL scaffold when treated with growth factors (**F1,** cell crystal violet staining; **F2,** semiquantitative analysis of the intensity of crystal violet, n=3, two-way ANOVA). **(G)** The assessment of GAG deposition in human synovium-derived MSCs seeded onto PCL scaffold when treated with growth factors (**G1,** alcian staining; **G2,** semiquantitative analysis of GAG deposition, n=5, two-way ANOVA). **(H)** The assessment of COL I, COL II, SOX9 expression in human synovium-derived MSCs seeded onto PCL scaffold when treated with growth factors (**H1,** cell immunofluorescence; **H2,** semiquantitative analysis, n=3, two-way ANOVA). **(I)** The immunofluorescent assessment of TGFβ1, CTGF in regenerated tissue and native porcine menisci (**I1,** 2 months postoperatively; **I2,** 4 months postoperatively; **I3,** native porcine menisci; **I4,** semiquantitative analysis of TGFβ1, CTGF; n=6 for 2M and 4M groups; n=3 for native menisci; two-way ANOVA).

(J) The immunofluorescent assessment of pSmad2/3 in regenerated tissue and native porcine menisci. **(K)** The immunofluorescent assessment of pSmad2/3 in porcine synovium (**K1,** tissue immunofluorescence; **K2,** semiquantitative analysis, n=4, one-way ANOVA).

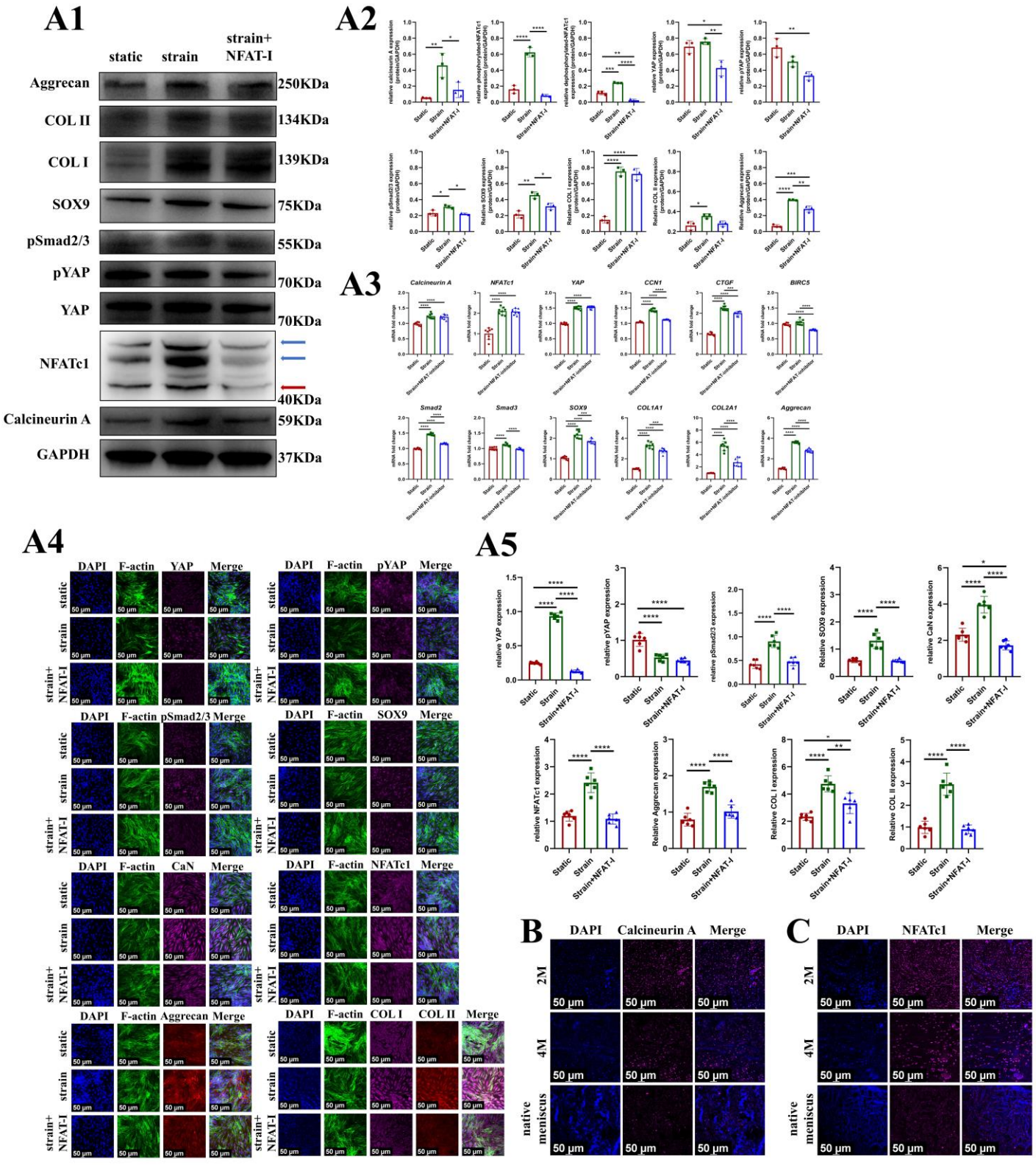
A1
static
strain
strain+ NFAT-I
Aggrecan
COL II
COL I
SOX9
pSmad2/3
pYAP
YAP
NFATc1
Calcineurin A
GAPDH
250KDa
134KDa
139KDa
75KDa
55KDa
70KDa
70KDa
40KDa
59KDa
37KDa
A2
A3
A4
DAPI
F-actin
YAP
pYAP
pSmad2/3
SOX9
CaN
NFATc1
Aggrecan
COL I
COL II
Merge
50 μm
A5
relative YAP expression
relative pYAP expression
relative pSmad2/3 expression
Relative SOX9 expression
relative CaN expression
relative NFATc1 expression
Relative Aggrecan expression
Relative COL I expression
Relative COL II expression
Static
Strain
Strain+NFAT-I
B
Calcineurin A
2M
4M
native meniscus
C
NFATc1

Supplemental figure 23. The protein and mRNA levels in human synovium-derived MSCs after treated with CTS or NFAT inhibitor (NFAT-I). The expression of calcineurin and NFATc1 in regenerated tissue of PCL scaffold+synovium transplant group and native porcine menisci. (A) The protein and mRNA levels in human synovium-derived MSCs after treated with CTS or NFAT inhibitor (**A1,** the western blot analysis; **A2,** the semiquantitative analysis of western blot, n=3, one-way ANOVA; **A3,** the mRNA levels, n=8, one-way ANOVA; **A4,** cell immunofluorescence, CaN: calcineurin A; **A5,** the semiquantitative analysis of immunofluorescence, n=6, one-way ANOVA). **(B)** the immunofluorescence of calcineurin in regenerated tissue of PCL scaffold+synovium transplant group and native porcine menisci. **(C)** the immunofluorescence of NFATc1 in regenerated tissue of PCL scaffold+synovium transplant group and native porcine menisci.

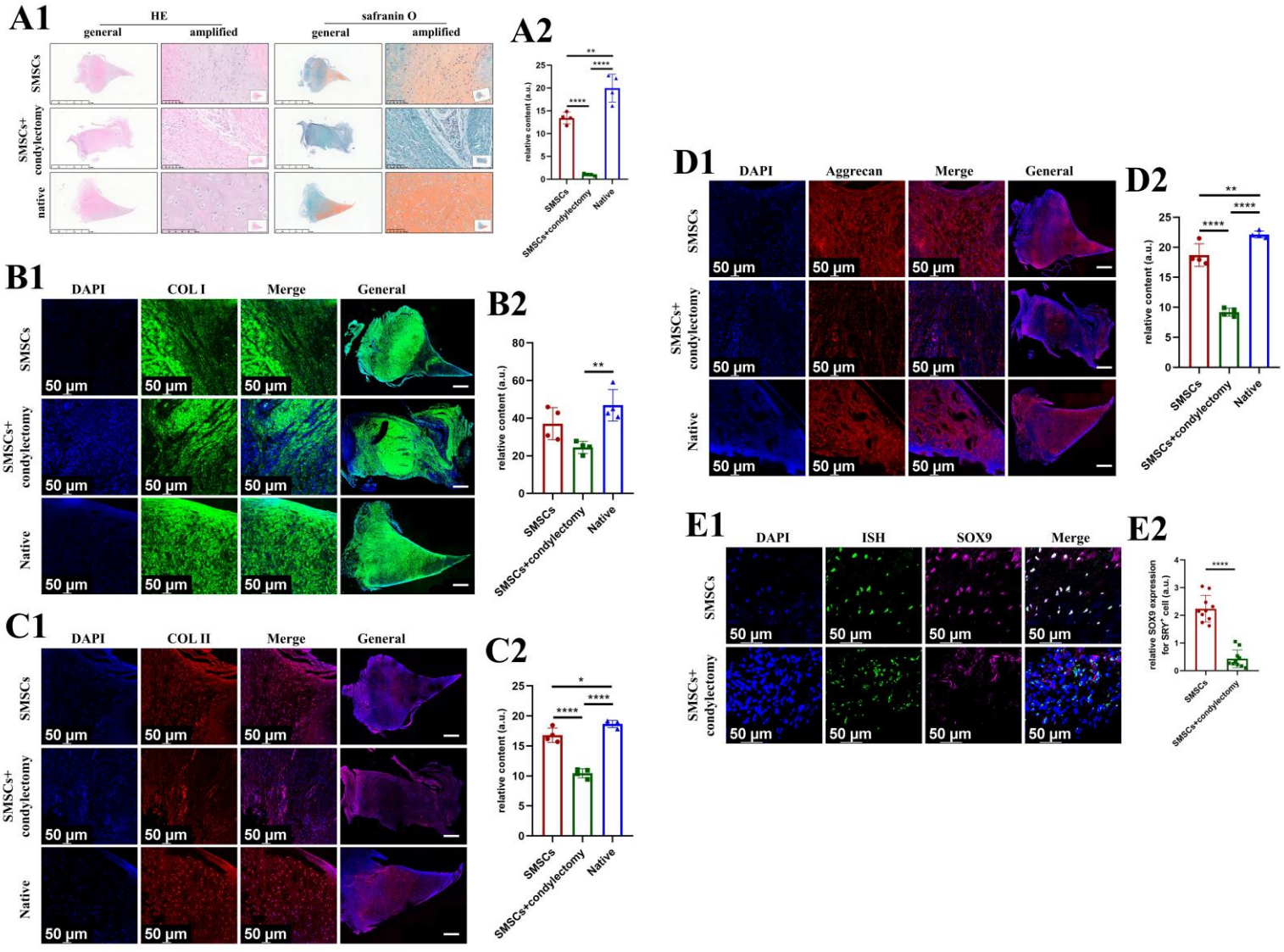
A1
HE
safranin O
general
amplified
general
amplified
SMSCs
SMSCs+ condylectomy
native
A2
relative content (a.u.)
SMSCs
SMSCs+condylectomy
Native
B1
DAPI
COL I
Merge
General
SMSCs
SMSCs+ condylectomy
Native
50 μm
B2
relative content (a.u.)
SMSCs
SMSCs+condylectomy
Native
C1
DAPI
COL II
Merge
General
SMSCs
SMSCs+ condylectomy
Native
50 μm
C2
relative content (a.u.)
SMSCs
SMSCs+condylectomy
Native
D1
DAPI
Aggrecan
Merge
General
SMSCs
SMSCs+ condylectomy
Native
50 μm
D2
relative content (a.u.)
SMSCs
SMSCs+condylectomy
Native
E1
DAPI
ISH
SOX9
Merge
SMSCs
SMSCs+ condylectomy
50 μm
E2
relative SOX9 expression for SRY+ cell (a.u.)
SMSCs
SMSCs+condylectomy

Supplemental figure 24. Mechanical deprivation affects chondrogenesis of transplanted allogenic rabbit synovium-derived MSCs and subsequent meniscal defect repair in a rabbit model at 4 weeks after operation. (A) The HE and safranin O staining of regenerated tissue in SMSCs transplant group, SMSCs transplant+condylectomy group, and native rabbit meniscus (**A1,** histological staining; **A2,** the semiquantitative analysis of GAG, n=4, one-way ANOVA). **(B)** the immunofluorescence of COL I of regenerated tissue and native meniscus (**B1,** the immunofluorescence of COL I, scale bar, 0.5 mm; **B2,** the semiquantitative analysis of COL I, n=4, one-way ANOVA). **(C)** the immunofluorescence of COL II of regenerated tissue and native meniscus (**C1,** the immunofluorescence of COL II, scale bar, 0.5 mm; **C2,** the semiquantitative analysis of COL II, n=4, one-way ANOVA). **(D)** the immunofluorescence of Aggrecan of regenerated tissue and native meniscus (**D1,** the immunofluorescence of Aggrecan, scale bar, 0.5 mm; **D2,** the semiquantitative analysis of Aggrecan, n=4, one-way ANOVA). **(E)** condylectomy affects the chondrogenesis of transplanted SMSCs (**E1,** the colocalization of SOX9 immunofluorescence and in situ hybridization for SRY gene in SMSCs transplant group and SMSCs transplant+condylectomy group; **E2,** the semiquantitative analysis of SOX9 expression for SRY positive cells, n=10, unpaired *t*-test).

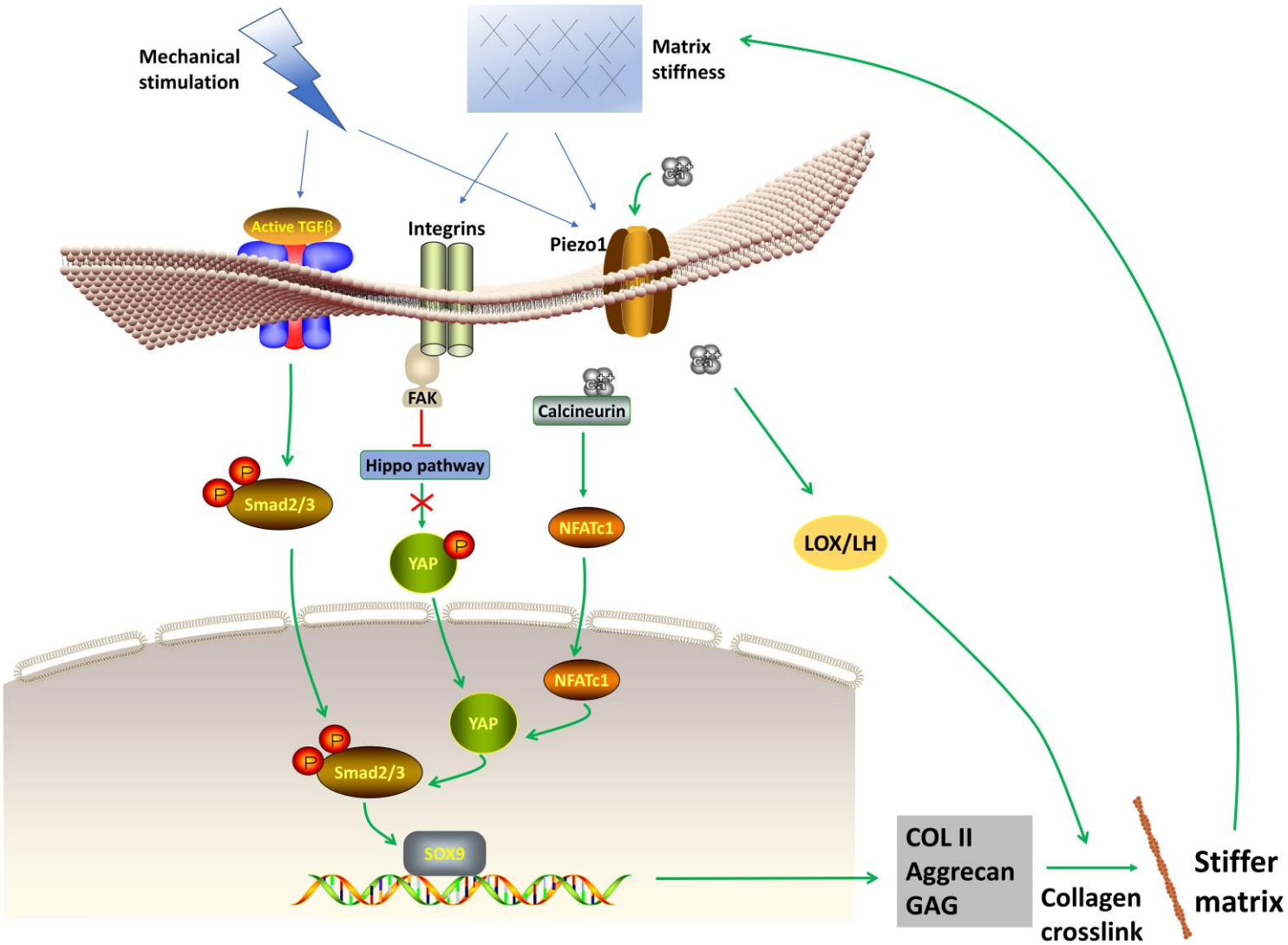
Mechanical stimulation
Matrix stiffness
Active TGFβ
Integrins
Piezo1
Ca2+
FAK
Calcineurin
Hippo pathway
Smad2/3
YAP
NFATc1
LOX/LH
SOX9
COL II
Aggrecan
GAG
Collagen crosslink
Stiffer matrix

Supplemental figure 25. The molecular mechanisms of synovium-derived MSCs chondrogenesis at the condition of biomechanical, biochemical and matrix stiffness stimulus.

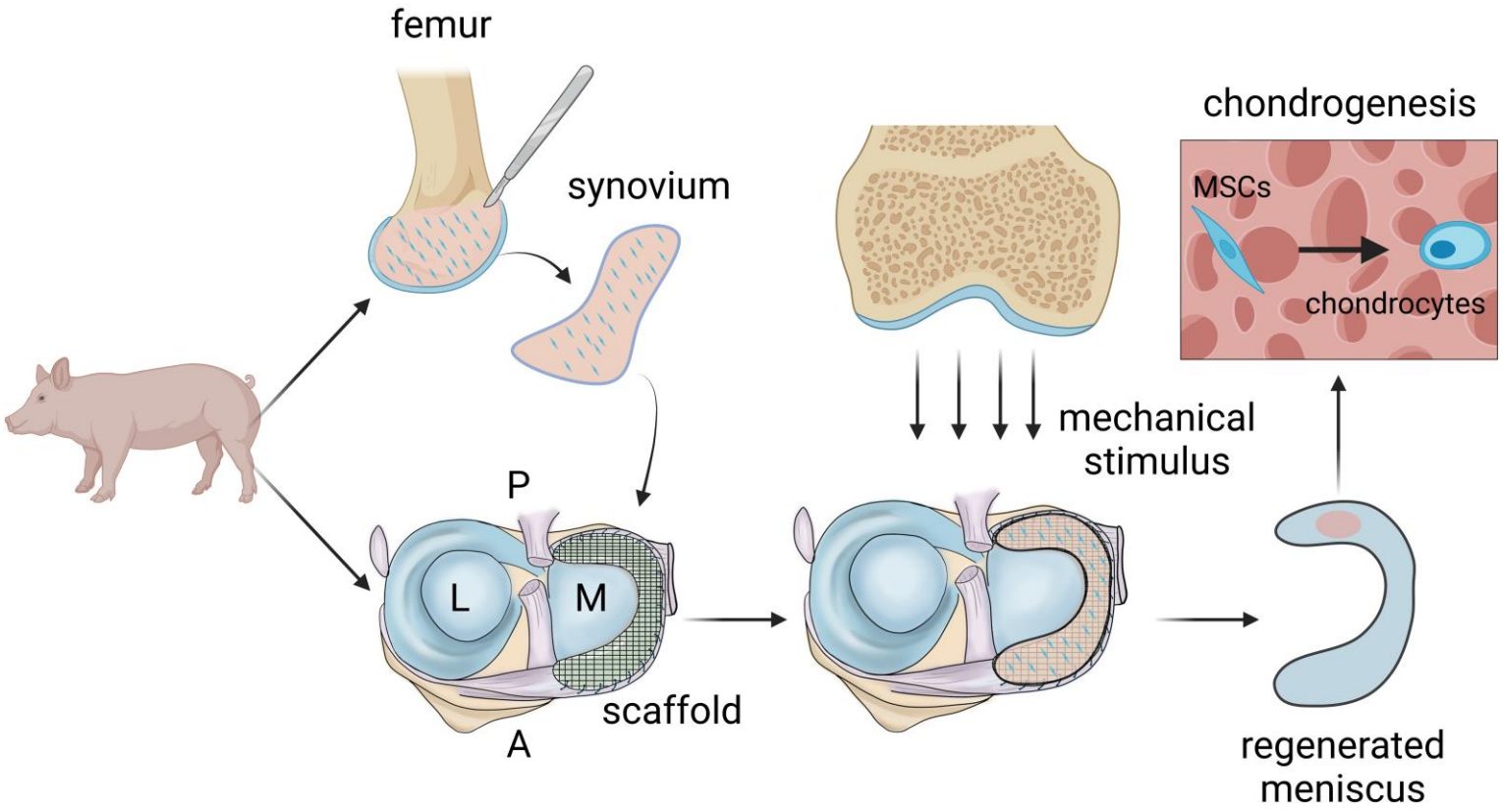
femur
synovium
chondrogenesis
MSCs
chondrocytes
mechanical
stimulus
P
L
M
A
scaffold
regenerated
meniscus

Supplemental figure 26. The schematics diagram of 3D printed PCL scaffold implant combining autologous synovium transplant on facilitating meniscal fibrocartilage regeneration. A: anterior; P: posterior; M: medial; L: lateral.

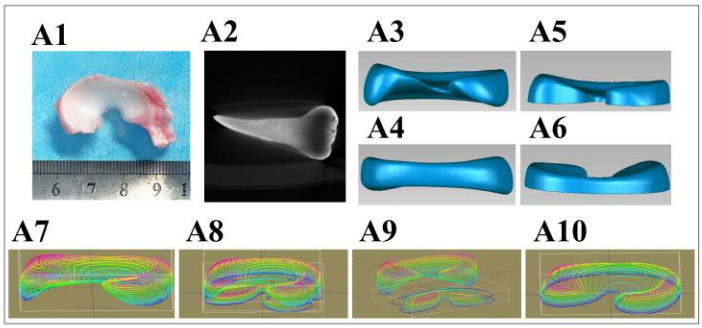
A1
A2
A3
A5
A4
A6
A7
A8
A9
A10

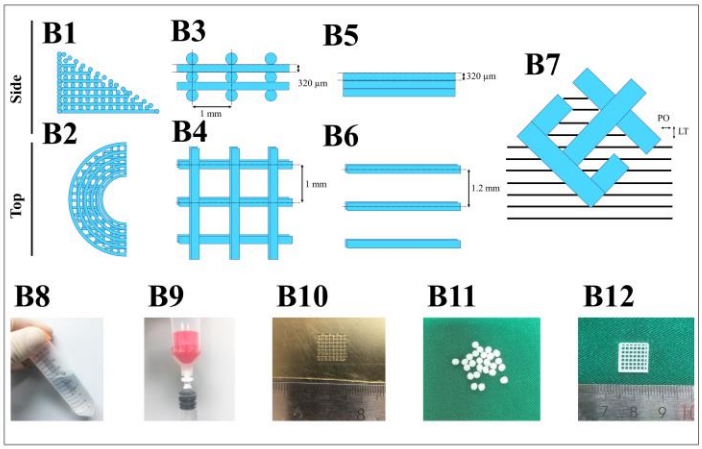
B1
B3
B5
B7
Side
B2
B4
B6
Top
320 μm
1 mm
1.2 mm
PO
LT
B8
B9
B10
B11
B12

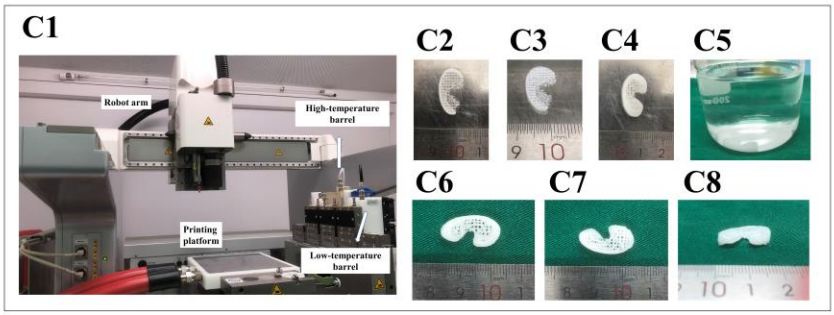
C1
Robot arm
High-temperature barrel
Printing platform
Low-temperature barrel
C2
C3
C4
C5
C6
C7
C8

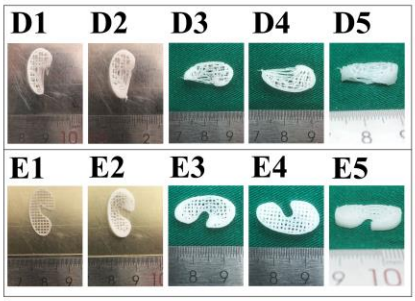
D1
D2
D3
D4
D5
E1
E2
E3
E4
E5


F

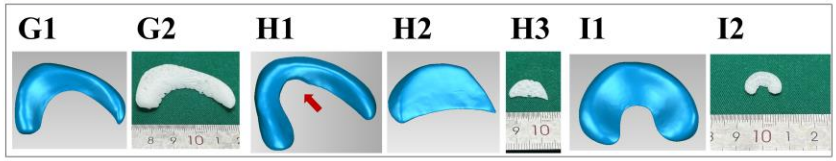
G1
G2
H1
H2
H3
I1
I2

Supplemental figure 27. 3D printing PCL meniscal scaffold. (A) The construction of meniscal 3D printing model (**A1,** native porcine meniscus; **A2,** micro-CT scanning image of native meniscus; **A3,** native meniscal 3D model-inner view; **A4,** native meniscal 3D model-outer view; **A5,** meniscal 3D model with flat bottom-inner view; **A6,** meniscal 3D model with flat bottom-outer view; **A7,** uniform slicing of native meniscal main subject printing model; **A8,** uniform slicing of native meniscal main subject printing model and supporting structure printing model-assembly; **A9,** uniform slicing of native meniscal main subject printing model and supporting structure printing model-divided; **A10,** uniform slicing of meniscal printing model with flat bottom). **(B)** The schematics of printing strand design and the preparation of printing materials (**B1,** printing strand in each layer-side view; **B2,** printing strand in each layer-top view; **B3,** the inner structure of the meniscal main subject printing model-side view; **B4,** the inner structure of the meniscal main subject printing model-top view; **B5,** the inner structure of supporting printing model-side view; **B6,** the inner structure of supporting printing model-top view; **B7,** the schematics of supporting printing, PO, polygon offset, LT, layer thickness; **B8,** 30% w/v Pluronic F-127 solution; **B9,** the Pluronic F-127 solution is injected into low-temperature material barrel through a bipass; **B10,** the printability of Pluronic F-127 under optimal printing conditions; **B11,** PCL pellets; **B12,** the printability of PCL under optimal printing conditions). **(C)** The construction of native meniscal scaffold using supporting printing (**C1,** the Bioplotter printing machine; **C2-C3,** layer-by-layer printing process, the bottom transparent lines represent Pluronic F-127; **C4,** the final product of supporting printing meniscal scaffold; **C5,** the meniscal

scaffold is immersed into water to remove extra Pluronic F-127; **C6-C8,** the photographs of native meniscal scaffold from different views). **(D)** The printing of native meniscal scaffold without supporting structure (**D1-D2,** layer-by-layer printing process; **D3-D5,** the photographs of scaffold from different views). **(E)** The printing of meniscal scaffold with flat bottom (**E1-E2,** layer-by-layer printing process; **E3-E5,** the photographs of scaffold from different views). **(F)** The comparison of supporting printing native meniscal scaffold and scaffold with flat bottom. **(G)** Supporting printing scaffold of the whole human medial meniscus (**G1,** 3D model of human meniscus; **G2,** human meniscal scaffold). **(H)** Supporting printing scaffold of partial meniscal defect in human meniscus (**H1,** meniscal 3D model showing the defect is created in the posterior horn of meniscus, the red arrowhead represents defect site; **H2,** 3D model of meniscal defect; **H3,** scaffold of meniscal defect). **(I)** Supporting printing scaffold of beagle canine medial meniscus (**I1,** 3D model of beagle canine meniscus; **I2,** beagle canine meniscal scaffold).

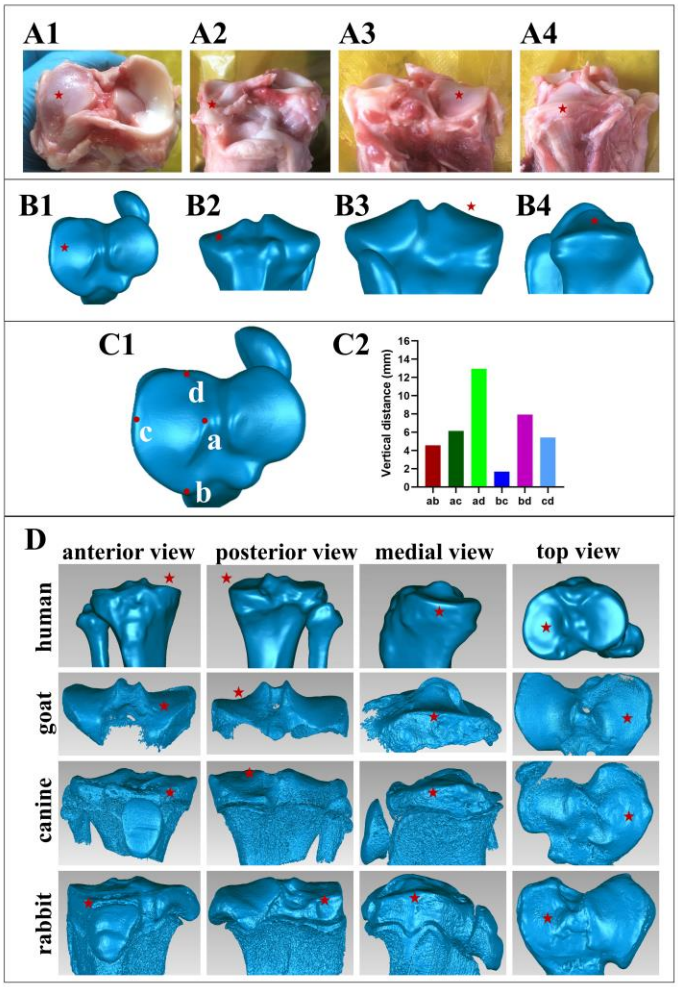
A1
A2
A3
A4
B1
B2
B3
B4
C1
d
c
a
b
C2
Vertical distance (mm)
16
14
12
10
8
6
4
2
0
ab
ac
ad
bc
bd
cd
D
anterior view
posterior view
medial view
top view
human
goat
canine
rabbit

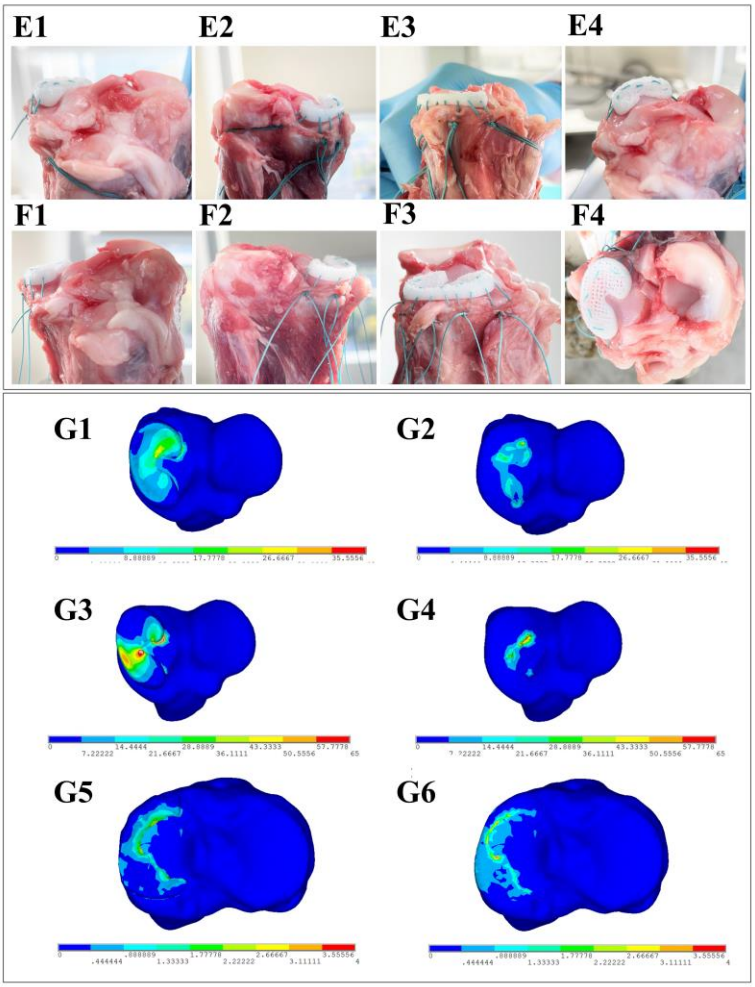
E1
E2
E3
E4
F1
F2
F3
F4
G1
G2
G3
G4
G5
G6

Supplemental figure 28. The characterization of tibial plateau, the transplantation of meniscal scaffold, the finite element analysis of compression distribution in meniscus and tibial plateau. (A) The gross anatomy of porcine tibial plateau evaluated from different views (**A1,** top view; **A2,** anterior view; **A3,** posterior view; **A4,** medial view, the red five-pointed star represents medial tibial plateau). **(B)** The 3D model of porcine tibial plateau evaluated from different views (**B1,** top view; **B2,** anterior view; **B3,** posterior view; **B4,** medial view, the red five-pointed star represents medial tibial plateau). **(C)** The quantitative assessment of medial tibial plateau (**C1,** the identification of peripheral rim of medial tibial plateau, a: lateral rim, b: anterior rim, c: medial rim, d: posterior rim; **C2,** the vertical distances among a, b, c, d points). **(D)** The 3D model of tibial plateau of other species, including human, goat, canine, rabbit, evaluated from different views. The red five-pointed star represents medial tibial plateau. **(E)** Supporting printing meniscal scaffold is transplanted to the tibial plateau specimen and photographed from different views (**E1,** anterior view; **E2,** posterior view; **E3,** medial view; **E4,** top view); **(F)** Flat-bottom meniscal scaffold is transplanted to the tibial plateau specimen and photographed from different views (**F1,** anterior view; **F2,** posterior view; **F3,** medial view; **F4,** top view); **(G)** The finite element analysis of compression distribution in meniscus and tibial plateau (**G1,** medial meniscus of native porcine meniscal model; **G2,** medial tibial plateau of native porcine meniscal model; **G3,** medial meniscus of flat bottom porcine meniscal model; **G4,** medial tibial plateau of flat bottom porcine meniscal model; **G5,** medial meniscus of native human knee joint; **G6,** medial tibial plateau of native human knee joint).

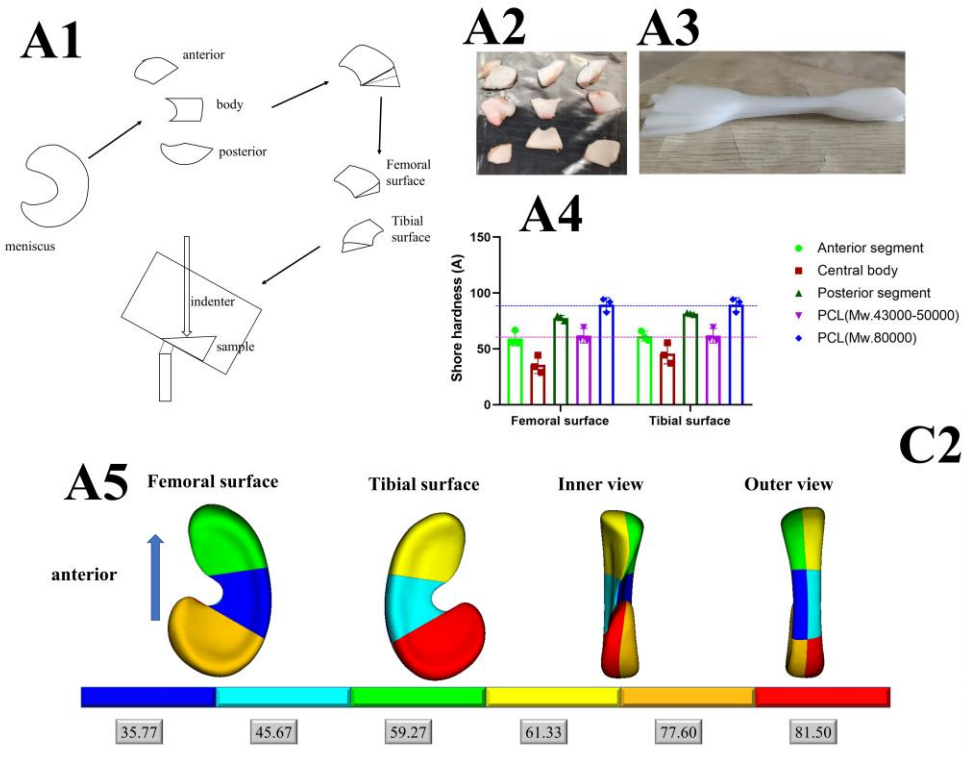
A1
anterior
body
posterior
meniscus
Femoral surface
Tibial surface
indenter
sample
A2
A3
A4
Shore hardness (A)
150
100
50
0
Femoral surface
Tibial surface
Anterior segment
Central body
Posterior segment
PCL(Mw.43000-50000)
PCL(Mw.80000)
C1
C2
A5
Femoral surface
Tibial surface
Inner view
Outer view
anterior
35.77
45.67
59.27
61.33
77.60
81.50
B1
Bottom
Surface
Anterior horn
Body
Posterior horn
Cross section
Anterior horn
Posterior horn
Body
B2
Surface
Bottom
Cross section
Anterior horn
Body
Posterior horn

Supplemental figure 29. The characterization of mechanical property, inner structure and biocompatibility of PCL scaffold. (A) Shore hardness testing of native porcine meniscus and PCL (**A1,** the schematics of sample preparation and testing; **A2,** the dissected porcine medial meniscus sample; **A3,** the dumbbell-shaped PCL sample; **A4,** the results of shore hardness testing, the dotted lines represent the mean values of PCL of two different molecular weights. n=3; **A5,** heat map of shore hardness distribution in native porcine meniscus, the values below color strips represent mean values of shore hardness in the corresponding section of porcine menisci). **(B)** The SEM characterization of supporting printing meniscal scaffold (**B1,** sample preparation before SEM observation; **B2,** the SEM characterization of scaffold showing the surface, bottom, cross section of anterior horn, central body, posterior horn, respectively). **(C)** The cytocompatibility of PCL scaffold (**C1,** live-dead staining of cells seeded onto PCL scaffold, green fluorescence represents live cells, red fluorescence represents dead cells; **C2,** the cytoskeleton of cells, green fluorescence represents cytoskeleton, blue fluorescence represents nucleus).

The following tables are provided as separate Excel files

Supplemental table 1. Abbreviations used.

Supplemental table 2. Key resources table.

Supplemental table 3. The information of porcine used in the present study.

Supplemental table 4. Primer sequences for human synovium-derived MSCs.

Supplemental table 5: raw data of Fig. 3B8

Supplemental table 6: statistical significance of Fig. 3B8

Supplemental table 7: raw data of Fig. 4E2

Supplemental table 8: statistical significance of Fig. 4E2

Supplemental table 9: raw data of Fig. 4E3

Supplemental table 10: statistical significance of Fig. 4E3

Supplemental table 11: raw data of Fig. 4F2

Supplemental table 12: statistical significance of Fig. 4F2

Supplemental table 13: raw data of Fig. 5A2

Supplemental table 14: statistical significance of Fig. 5A2

Supplemental table 15: raw data of Fig. 5A4

Supplemental table 16: statistical significance of Fig. 5A4

Supplemental table 17: raw data of Fig. 5A6

Supplemental table 18: statistical significance of Fig. 5A6

Supplemental table 19: raw data of Fig. 5A7

Supplemental table 20: statistical significance of Fig. 5A7

Supplemental table 21: raw data of Fig. 5B2, C2

Supplemental table 22: raw data of Fig. 6A2, A4, A5

Supplemental table 23: statistical significance of Fig. 6A2, A4, A5

Supplemental table 24: raw data of Fig. 6C2

Supplemental table 25: statistical significance of Fig. 6C2

Supplemental table 26: raw data of Fig. 6C3

Supplemental table 27: statistical significance of Fig. 6C3

Supplemental table 28: raw data of Fig. 6C5

Supplemental table 29: statistical significance of Fig. 6C5

Supplemental table 30: raw data of Fig. 6C7

Supplemental table 31: statistical significance of Fig. 6C7

Supplemental table 32: raw data of Fig. 6D2, D4

Supplemental table 33: statistical significance of Fig. 6D2, D4

Supplemental table 34: raw data of Fig. 6E2

Supplemental table 35: statistical significance of Fig. 6E2

Supplemental table 36: raw data of Fig. 6E4

Supplemental table 37: statistical significance of Fig. 6E4

Supplemental table 38: raw data of Fig. 6E5

Supplemental table 39: statistical significance of Fig. 6E5

Supplemental table 40: raw data of Fig. 6E7

Supplemental table 41: statistical significance of Fig. 6E7

Supplemental table 42: raw data of Fig. 7A1

Supplemental table 43: raw data of Fig. 7A3

Supplemental table 44: statistical significance of Fig. 7A3

Supplemental table 45: raw data of Fig. 7A5

Supplemental table 46: statistical significance of Fig. 7A5

Supplemental table 47: raw data of Fig. 7A6

Supplemental table 48: statistical significance of Fig. 7A6

Supplemental table 49: raw data of Fig. 7B2, C2

Supplemental table 50: statistical significance of Fig. 7B2, C2

Supplemental table 51: raw data of Fig. 8A2, A3, A5, A7, A8

Supplemental table 52: statistical significance of Fig. 8A2, A3, A5, A7, A8

Supplemental table 53: raw data of Fig. 8B2, B3, B5, B7, B8

Supplemental table 54: statistical significance of Fig. 8B2, B3, B5, B7, B8

Supplemental table 55: raw data of Fig. 8C2, C3, C4

Supplemental table 56: statistical significance of Fig. 8C2, C3, C4

Supplemental table 57: raw data of supplemental Fig. 9

Supplemental table 58: statistical significance of supplemental Fig. 9

Supplemental table 59: raw data of supplemental Fig. 10

Supplemental table 60: statistical significance of supplemental Fig. 10

Supplemental table 61: raw data of supplemental Fig. 18

Supplemental table 62: statistical significance of supplemental Fig. 18

Supplemental table 63: raw data of Fig. 19B

Supplemental table 64: statistical significance of Fig. 19B

Supplemental table 65: raw data of supplemental Fig. 20A2

Supplemental table 66: statistical significance of supplemental Fig. 20A2

Supplemental table 67: raw data of supplemental Fig. 20C1-C3

Supplemental table 68: statistical significance of supplemental Fig. 20C1-C3

Supplemental table 69: raw data of supplemental Fig. 20F2

Supplemental table 70: statistical significance of supplemental Fig. 20F2

Supplemental table 71: raw data of supplemental Fig. 21A2

Supplemental table 72: statistical significance of supplemental Fig. 21A2

Supplemental table 73: raw data of supplemental Fig. 21B3

Supplemental table 74: statistical significance of supplemental Fig. 21B3

Supplemental table 75: raw data of supplemental Fig. 22A2, B2

Supplemental table 76: statistical significance of supplemental Fig. 22A2, B2

Supplemental table 77: raw data of supplemental Fig. 22E2

Supplemental table 78: statistical significance of supplemental Fig. 22E2

Supplemental table 79: raw data of supplemental Fig. 22F2, G2, H2

Supplemental table 80: statistical significance of supplemental Fig. 22F2, G2, H2

Supplemental table 81: raw data of supplemental Fig. 22I4

Supplemental table 82: statistical significance of supplemental Fig. 22I4

Supplemental table 83: raw data of supplemental Fig. 22K2

Supplemental table 84: statistical significance of supplemental Fig. 22K2

Supplemental table 85: raw data of supplemental Fig. 23A2

Supplemental table 86: statistical significance of supplemental Fig. 23A2

Supplemental table 87: raw data of supplemental Fig. 23A3

Supplemental table 88: statistical significance of supplemental Fig. 23A3

Supplemental table 89: raw data of supplemental Fig. 23A5

Supplemental table 90: statistical significance of supplemental Fig. 23A5

Supplemental table 91: raw data of supplemental Fig. 24A2, B2, C2, D2, E2

Supplemental table 92: statistical significance of supplemental Fig. 24A2, B2, C2, D2, E2

Supplemental table 93: raw data of supplemental Fig. 29A4

Supplemental Movie 1. The biomimetic meniscal scaffold with native bottom morphology was attempted using supporting printing.

Supplemental Movie 2. The meniscal model with native bottom morphology was attempted without supporting model.

Supplemental Movie 3. The meniscal scaffold with flat bottom was printed.

Supplemental Movie 4. The gait analysis of minipig after transplantation at 2 months postoperatively.

Supplemental Movie 5. The gait analysis of minipig after transplantation at 4 months postoperatively.